Euro. Jnl of Applied Mathematics (2009), *vol.* 20, *pp.* 363–397.
doi:10.1017/S0956792509007839 Printed in the United Kingdom

A Survey in Mathematics for Industry
A review of computational fluid dynamics analysis of blood pumps

M. BEHBAHANI[1], M. BEHR[1], M. HORMES[2], U. STEINSEIFER[2], D. ARORA[3], O. CORONADO[3] and M. PASQUALI[3]

[1]*Center for Computational Engineering Science, RWTH Aachen, 52056 Aachen, Germany*
(*email*: mb@cats.rwth-aachen.de; behr@cats.rwth-aachen.de)
[2]*Department of Cardiovascular Engineering, Helmholtz Institute, 52056 Aachen, Germany*
(*email*: Hormes@hia.rwth-aachen.de; steinseifer@hia.rwth-aachen.de)
[3]*Department of Chemical and Biomolecular Engineering, Rice University, Houston, TX 77005, USA*
(*email*: dhruv@alumni.rice.edu; ocm@alumni.rice.edu; mp@rice.edu)

(*Received 1 March 2007; revised 22 January 2009; first published online 6 March 2009*)

Ventricular assist devices (VADs) provide long- and short-term support to chronically ill heart disease patients; these devices are expected to match the remarkable functionality of the natural heart, which makes their design a very challenging task. Blood pumps, the principal component of the VADs, must operate over a wide range of flow rates and pressure heads and minimise the damage to blood cells in the process. They should also be small to allow easy implantation in both children and adults. Mathematical methods and computational fluid dynamics (CFD) have recently emerged as powerful design tools in this context; a review of the recent advances in the field is presented here. This review focusses on the CFD-based design strategies applied to blood flow in blood pumps and other blood-handling devices. Both simulation methods for blood flow and blood damage models are reviewed. The literature is put into context with a discussion of the chronological development in the field. The review is illustrated with specific examples drawn from our group's Galerkin/least squares (GLS) finite-element simulations of the basic Newtonian flow problem for the continuous-flow centrifugal GYRO blood pump. The GLS formulation is outlined, and modifications to include models that better represent blood rheology are shown. Haemocompatibility analysis of the pump is reviewed in the context of haemolysis estimations based on different blood damage models. Our strain-based blood damage model that accounts for the viscoleasticity associated with the red blood cells is reviewed in detail. The viability of design improvement based on trial and error and complete simulation-based design optimisation schemes are also discussed.

1 Introduction

Computational fluid dynamics (CFD) has made impressive progress in the past decade and has evolved into a promising design tool for the development of biomedical devices. This paper focusses on the evolution and current state of analysis of ventricular assist devices (VADs) that support the circulatory system of patients suffering from heart failure (HF), which is the most common fatal disease in developed countries. Due to the permanent shortage of donor hearts available for transplantation, VADs are often the last hope for end-stage HF patients; these devices can now provide circulatory support for periods

up to two years [99]. The blood pump is the key component of a VAD system, and its design has greatly benefited from CFD; however, the design of blood pumps still presents significant challenges.

The main function of a blood pump is to deliver adequate hydraulic performance while maintaining good haematological compatibility. Hydraulic performance implies the pump's ability to generate a desired flux at a given pressure head (resistance); haematological requirements arise because non-physiological flow conditions in a pump often lead to haemolysis (haemoglobin release from red blood cells or RBCs) and thrombosis (clotting of blood). Haemolysis beyond a certain level and thrombosis are the two major life risk factors for patients who depend on a VAD. CFD is an excellent analysis tool to deliver detailed insight into the complex patterns of blood flow that determine hydraulic performance. Moreover, in combination with an adequate blood damage model, CFD allows quantitative prediction of haemolysis. It also supports the engineer in identifying recirculation areas and other regions with an increased probability for blood clotting.

This paper reviews the research in haemodynamics and blood damage analysis. The presented numerical examples are based on the numerical approaches employed by the authors' research groups and applied to the simulation of the GYRO centrifugal pump, under development at Baylor College of Medicine. Statistics pertaining to HF are discussed in Section 2. Section 3 describes existing types of VADs; the role of CFD in their design process is analysed in Section 4. The rheology of blood and some constitutive models that endeavour to represent the complex flow behaviour of blood are described in Section 5. Section 6 reviews numerical flow analysis, where blood is considered as an idealised Newtonian fluid. The mathematical models for haemolysis are reviewed in Section 7. Section 8 describes the numerical solution for the flow of blood modelled as a viscoelastic Oldroyd-B fluid. Aspects of an automatic design optimisation are described in Section 9. In Section 10, we conclude with some future directions for the developments in the field.

2 Heart failure

HF is a clinical syndrome that implies dysfunction of the heart's ventricle and a limited cardiac performance. HF develops gradually as the heart muscle weakens and causes an imbalance in pump function; i.e. the heart fails to maintain adequate blood circulation. The term congestive heart failure (CHF) is used if the reduced pumping ability of the heart leads to the build-up of fluid in the lungs and other body tissues.

By 2004, more than 20 million people suffered from HF worldwide, and 2 million new cases are diagnosed each year [117]. The number of people afflicted with HF is particularly high in the developed countries due to higher life expectancy and older population. Nutritional lifestyle including excessive consumption of high-fat food leads to hyperlipidemia, which constitutes a further risk factor for accelerated atherosclerosis (formation of plaque in the walls of the arteries leading to narrowing of blood vessels) and ultimately HF [119]. In the United States of America alone, 5 million cases of HF were reported in 2002, and 550,000 new cases are reported every year [4]. About 1% of all newborns are afflicted with a debilitating congenital heart defect [75]. On average 49% of men and 32% of women over 40 years of age are at risk of developing HF [4], and it is the most prominent cause of hospitalisation for people aged above 65 [74]. Approximately

20% of the patients die in the first year after the diagnosis, and 70%–80% have life spans shorter than eight years. In 2003, 286,700 deaths in United States of America were caused by HF, representing one in every five deaths [4].

Heart transplant remains the only permanent treatment for end-stage patients; however, only 2,500 donor hearts become available each year, while 50,000 patients remain in waiting [51]. The waiting times for patients with an urgent need of heart transplant are normally longer than two years. Annually, care and treatment of HF patients costs the American health care system 29.6 billion dollars [4].

3 Ventricular assist devices

As evidenced by the statistics in Section 2, heart transplantation alone cannot suffice as a clinical solution for all HF patients; therefore, total artificial hearts (TAHs) as well as VADs are being increasingly used to provide support to the ailing heart and alleviate suffering. For brevity, this paper focusses only on computational analysis of VADs; the modelling and simulation issues are basically the same as those of TAHs, and distinction is blurring with new uses of paired VADs functioning as a TAH.

A VAD is defined as a *temporary* life-sustaining system which consists of a blood pump, a power supply and a control unit and is used to support the blood circulation by decreasing the workload of the heart while maintaining adequate blood pressure [99]. However, these devices are now being envisaged as permanent clinical solutions.

In 1966, a VAD was successfully implanted into a patient for the first time. In 1982, a Jarvik-7 artificial heart was implanted in a patient who survived on it for almost four months [51]. Since 1990, as new technologies gradually allowed for more efficient heart pumps, several companies started the development of VADs. In 1994, the US Food and Drug Administration (FDA) approved the left ventricular assist device (LVAD), i.e. VAD that specifically supports the work of the left ventricle, as a bridge to transplant. The 2001 Randomized Evaluation of Mechanical Assistance for the Treatment of Congestive Heart Failure (REMATCH) studied LVAD therapy for patients with endstage HF. It could be shown that the survival chances of the patients were twice as high if they were fitted with LVADs instead of merely receiving medical therapy [116]. In 2002, the FDA approved the use of LVADs for long-term therapy in severe HF patients, who cannot be candidates for heart transplants [89].

Anatomically, the VADs are implanted either internally in the abdomen (like DeBakey, HeartMate and Novacor) or in the pericardial space (like HeartWare HVAD), while in other cases, such as the pulsatile Thoratec VAD, the pump is placed extracorporeally. Takatani [130] listed more than 30 different heart pumps that have been in clinical use or under development until 2001. The cost of a single VAD is typically over 50,000 US dollars [8]; however, these devices have the potential to bring overall financial relief to the national health systems.

3.1 Current applications

Table 1 lists the different configurations in which VADs are used and their respective functions. Depending on whether VADs are connected to the left or right ventricle or

Table 1. *Configurations of mechanical circulatory support and their function*

Configuration	Function	Typical operating condition	Native heart
LVAD	Supports or replaces pumping function of heart's left ventricle	5 L min^{-1} at 100-mmHg aortic pressure	In place
RVAD	Supports or replaces pumping function of heart's right ventricle	4 L min^{-1} at 40-mmHg pulmonary pressure	In place
BIVAD	Supports or replaces pumping function of heart's both ventricles	5 L min^{-1} at 100-mmHg aortic pressure, 4 L min^{-1} at 40-mmHg pulmonary pressure	In place
TAH	Replaces the heart	5 L min^{-1} at 100-mmHg aortic pressure, 4 L min^{-1} at 40-mmHg pulmonary pressure	Removed

both ventricles, they are referred to as LVAD, right ventricular assist device (RVAD) or bi-ventricular assist device (BIVAD), respectively. These devices can also be used in a TAH configuration in which the diseased heart is replaced completely; however, VADs can be removed if the patient's heart recovers. The optimal operating conditions depend on physiological properties of the patient's cardiovascular system. An approach to quantify and parameterise the range of operating conditions is given in [146].

Based on suggested period of usage, the VADs can be classified into two-day, two-week, six-month, two-year and permanent models [98, 99]. Table 2 shows current blood pump models, their applications and associated requirements.

Commercially available VADs exist for short-term support, e.g. during critical surgeries, extracorporeal membrane oxygenation (ECMO) and percutaneous cardiopulmonary support (PCPS), as well as for medium- and long-term bridging support. A bridge to therapy and recovery is used to unload partially or completely the diseased heart. Patient studies have shown that by a prolonged support of the heart's pumping function after several months up to one year, apparent signs of the heart's natural recovery were diagnosed [98, 99]. After two years, the recovery due to ventricular unloading cannot be improved beyond the optimum [72]. The bridge to transplant requires a durability that matches the waiting time for a donor heart which is often more than two years. Permanently implantable blood pumps are currently in development.

3.2 Design requirements

The development of a blood pump has to satisfy several general requirements such as atraumatic behaviour, affordability, control feasibility, reliability, good implantability and applicability for different physiological demands varying from patient to patient [143]. Apart from such general requirements, different applications require different pump designs, each of which poses particular technical challenges as listed in Table 2. Often, design objectives oppose each other, and one design criterion is optimised to the detriment

Table 2. *Blood pump models, their application and associated requirements; 'X' indicates mandatory feature, and '(X)' indicates preferable feature*

Blood pump model	Typical application	Durability requirement	Hydraulic performance	Anti-thrombogenicity	Low sublethal cell damage	Small size	Without extra corporeal connection
Short-term: support during clinical high-risk operation	Support during extracorporeal cardiopulmonary bypass	Two days	X				
Short-term: support during transient cardiopulmonary failure	ECMO, PCPS, postcardiotomy cardiac failure	Two weeks	X	X			
Middle-term: bridge to therapy	Treatment of dilated cardiomyopathy	Six months	X	X	X	(X)	
Long-term: bridge to recovery	Support until recovery of the heart	Two years	X	X	X	X	(X)
Long-term: bridge to tranplant	Support until transplant	> Two years	X	X	X	X	(X)
Long-term: destination therapy	Permanent support	> Five years	X	X	X	X	X

of another one. For long-term bridging models, integration of the energy supply and control unit into the implanted device avoids inflammation of the tissue, a frequent complication occurring in patients using a VAD with extracorporeal connection.

As a blood-pumping device, the VAD has to be designed to provide

- adequate hydraulic performance assisting the physiological pumping and
- good haemocompatibility which implies minimal blood damage.

Blood damage can occur by either thrombosis or haemolysis. Anti-thrombogenicity and minimisation of haemolysis resulting from high shear stresses [97] are the most important haematological design features. The two primary damage mechanisms are explained briefly below.

Thrombosis

Thrombosis is the formation of a clot or thrombus and is initiated by the body's haemostatic mechanisms to prevent unnecessary bleeding. The processes that lead to clotting are complex and have been described in [48,61,144] and the references therein. The three primary factors can be summarised under the term Virchow's triad [139]: alterations in blood flow, abnormalities of the vascular wall and alterations in the constitution of blood. Therefore, inside VADs, regions of high shear stress, recirculation or stagnation and blood contacting surfaces with low haemocompatibility must be avoided. When the thrombus formation mechanism has been triggered by such non-physiological causes, it can lead to a pathologically high degree of clotting. If a thrombus forms on a surface of the VAD, it may compromise its function, and if it circulates as a free thrombus in the blood stream, it can occlude blood vessels in vital organs. These thromboembolic incidents count among the primary causes of death for patients with ventricular assist support.

Haemolysis

Haemolysis refers to premature RBC damage, and its indicator is the release of haemoglobin from the erythrocyte into the plasma. In artificial organs, mechanical damage resulting from high-shear-stress levels and exposure times to these stress levels are the main causes of haemoglobin release; contributions from other effects such as osmosis and chemical and thermal processes are negligible [12]. Modern atraumatic blood pump design can avoid catastrophic rupture of RBCs; however, sublethal RBC damage needs to be reduced for all middle- and long-term blood pump models. A more detailed explanation of haemolysis and the associated physical mechanisms is given in Section 5.3. Minor haemolysis can raise the level of haemoglobin in the blood to deteriorate the patient's condition. Moreover, a large concentration of plasma-free haemoglobin, which must be filtered by the kidneys, can cause kidney dysfunction [102] and multiple-organ failure.

3.3 Classification of VADs

From a technological point of view, VADs can be classified into three generations [101, 102]; the characteristics, advantages and disadvantages of each of them are summarised in Table 3.

Table 3. *Classification of VADs*

VAD	Pump type	Characteristic design features	Advantages	Disadvantages
First generation	Positive-displacement, pulsatile flow	Valve system, large number of components	More physiological (pulsatile) condition	Large size, low durability, low reliability, thrombogenic
Second generation	Rotary, non-pulsatile, continuous flow	Spinning impeller, bearings and/or seals in direct contact with blood	Compactness, atraumatic behaviour, anti-thrombogenicity	Sealing issues, leakage issues
Third generation	Rotary, non-pulsatile, continuous flow	Only a single moving component, spinning impeller, magnetic bearings	Compactness, atraumatic behaviour, anti-thrombogenicity	Complex manufacturing process

First-generation blood pumps are positive-displacement or pulsatile pumps. In the 1980s, *in vivo* studies [92, 131, 158] gave evidence that animals could survive for a long period of time in an entirely depulsed state, proving that pulsatile blood flow does not represent a necessarily physiological condition. Until today, the debate continues among investigators on whether pulsatile mechanical support provides any substantial benefit to the patient by reproducing the natural heart beat and blood flow. Ündar [137] lists different aspects of pulsatile compared to non-pulsatile perfusion.

Second-generation blood pumps are non-pulsatile pumps. They are characterised by the use of a spinning impeller providing a continuous blood flow. Typically, second-generation VADs use contact bearings and/or seals, where the bearings are immersed in the blood stream or separated from the stream by seals.

The transition from second- to third-generation rotary blood pumps is characterised by magnetic bearings allowing the impeller to be suspended. The work by Wood *et al.* [143] and the references therein argue that the third-generation systems are at present the leading technology in the development of mechanical circulatory support.

3.4 Rotary blood pumps

Rotary pumps can be classified into two categories – centrifugal and axial. The centrifugal pumps, e.g. GYRO pump, shown in Figure 1(a), can produce higher pressures at lower rotational speeds, whereas axial pumps, e.g. MicroMed DeBakey pump, shown in Figure 1(b), operate at higher speeds to build up the pressure head required for the desired flow rate [128]. Higher speeds may lead to high shear stresses and thus higher probability of blood damage. For this reason, centrifugal pumps provide 'gentler' flow conditions;

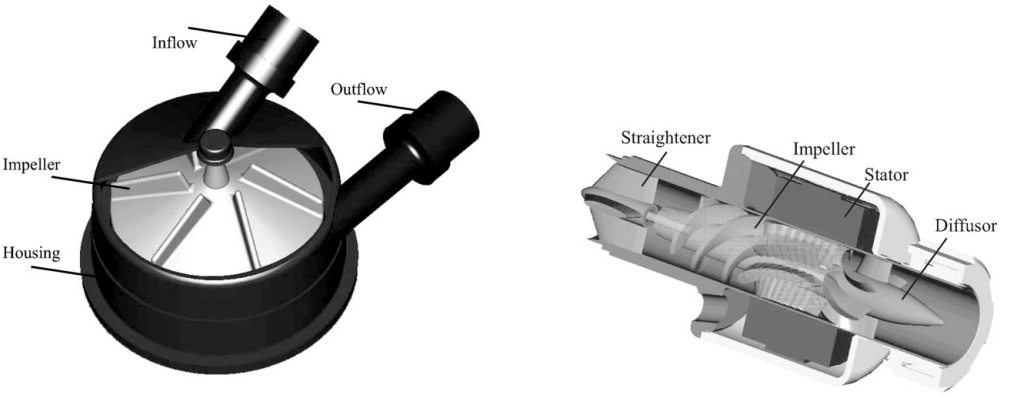

(a) GYRO pump (b) MicroMed DeBakey pump

FIGURE 1. (a) GYRO centrifugal pump and (b) MicroMed DeBakey axial pump. Image of the DeBakey pump courtesy of MicroMed Cardiovascular.

conversely, the shorter exposure times in axial pumps are expected to play a positive role. Advantageous applications of centrifugal pumps for VADs and other medical blood flow devices are described by Curtis [47]. Axial pumps are smaller and consume less power; therefore, they can be implanted more easily and are more suited for pediatric use. A description of nine of the most recent and established axial blood pump designs can be found in [125]. The particular pump design that is used in some of the numerical examples later in this paper is described below.

GYRO centrifugal pump

The GYRO centrifugal pump has been under development at the Baylor College of Medicine, Houston, Texas [96, 97, 157]. This pump has an impeller with six primary (top) and two secondary (bottom) vanes rotating inside a cylindrical pump housing. The bottom vanes are designed to create a secondary flow that increases bottom bearing washout. A double-pivot bearing system is used in order to obtain a sealless pump casing. The pump has a diameter of 6.5 cm and a priming volume of 25 mL. The inflow cannula is attached to the upper housing surface, and the outflow cannula is attached horizontally to the pump casing, both with a diameter of 0.8 cm. The inflow is positioned eccentrically in the vicinity of the top bearing in order to generate additional flow around the top shaft with the purpose of further reducing stagnant regions. Under typical operating conditions, the GYRO pump produces a flow of 5 L min^{-1} against 100-mmHg pressure at a rotor speed of 2,000 rpm.

4 Design tools for blood pumps

4.1 Experimental design tools

Flow visualisation techniques, *in vitro* and *in vivo* testing, have been traditionally used to analyse hydraulic and haematologic blood pump features.

Hydraulic testing is mainly performed using particle image velocimetry (PIV) [18, 49] and particle tracking velocimetry (PTV) [132, 141, 149, 150], which provide the velocity and stress fields. These techniques can be employed to confirm design expectations and to identify zones with a high potential for causing haemolysis or thrombus formation. One limitation of flow visualisation lies in its low resolution of critical areas, leading to low-fidelity predictions of flow characteristics in zones of particular interest. Generally, this difficulty is dealt with by performing the velocimetry in enlarged models, with associated scaling issues and problems. Another limitation is the need to perform the measurements in transparent models [18]. Finally, state-of-the-art visualisation methods do not allow the employment of blood as a working fluid during testing [132]. A promising future approach for measuring velocities of blood particles in blood pumps is the nuclear magnetic resonance (NMR) method [33]. The method allows the use of blood as the test fluid, and it has been applied to investigate blood flow in capillaries and tubes [69].

In vitro haematologic testing uses mock circulatory systems [83] which require large amounts of blood. Human blood is not easily available, and no equivalent artificial fluid has been produced so far; further restrictions on blood use for experiments are cited in [64]. As an alternative to human blood for mock tests, many experimental studies have used animal blood, which compared to human blood displays different behaviour in terms of rheological properties and mechanical fragility. All these factors exacerbate the difficulties of obtaining a reproducible and quantitatively adequate estimation of blood trauma based on *in vitro* testing.

In vivo studies are only able to give information about global design features, as the device is fully implanted in the living animal's circulatory system.

4.2 Numerical design tools

CFD made its methodical appearance in the field of heart pump development in the 1990s. CFD can be employed in the early stages of the design process as well as in later stages of optimisation. Nowadays, the design of medical devices involving blood flow, such as blood pumps, oxygenators and artificial heart valves, increasingly benefits from CFD modelling.

CFD represents a convenient and efficient tool for the analysis of hydraulic efficiency and flow patterns in the pump. It provides information such as the location and size of stagnation zones, local shear stress levels and exposure times of RBCs to such stresses; these parameters can then be correlated to the extent of haemolysis and thrombus formation. In the past decade, progress in blood modelling made CFD a powerful tool for the estimation of flow-induced blood damage. Based on haemolysis predictions, it is possible to perform pump optimisation according to blood-specific requirements.

The generally demanding computational resources for CFD studies are compensated by considerable advantages:

- CFD is time- and cost-effective because prototype building and experiments can be minimised;
- CFD can pinpoint the exact flow features inside the device; and
- modifications of the device model can be easily implemented.

5 Human blood

5.1 Blood as a complex and fragile fluid

Blood, which exhibits a highly complex, flow-dependent physical and chemical constitution, is composed of plasma, a Newtonian liquid of viscosity 1 mPa s, RBCs, white blood cells (WBCs) and platelets. Approximately 90% of the plasma is water, and the rest is composed of dissolved substances, primarily proteins, e.g. albumin, globulin and fibrinogen. The volume percentage of plasma typically accounts for 55%, and the remaining 45% is almost entirely composed of RBCs. Only up to 1% of the total cell mass in blood is formed by platelets and WBCs. Platelets are disc-shaped particles of 2–4 μm that are involved in the cellular mechanisms that initiate the wound-healing cascade through the formation of blood clots. The WBCs are responsible for the body's defense against infectious disease and foreign materials as part of the immune system. RBCs contain haemoglobin which has the function of distributing oxygen to the tissues and organs. Non-physiological conditions, in particular high shear stresses over a prolonged time, can cause damage to the RBCs. Characteristic shear stresses acting on blood in the human vessels as opposed to artificial organs are listed in [84]. These stresses lie within a range of 0.1–1 Pa in healthy human veins and 1–20 Pa in healthy human arteries, but this value can increase up to 50 Pa in narrowed arteries caused by stenotic lesions. In artificial blood pumps, typical values are found in a range of 1–1,000 Pa. Experimental evidence shows that in the practical range of exposure times (10 μs to 100 ms) RBCs are less resistant to shear than platelets [70]. The total characteristic residence time of a RBC in a VAD is of the order of 500 ms.

5.2 Red blood cells

RBCs are well adapted to resist shear stresses encountered under physiological conditions when blood is pumped through the network of narrow capillaries. When no external force acts on the membrane, an RBC takes the shape of an axisymmetric, biconcave, disc-like body. Its dimensions are determined by the elastic properties of the membrane, its surface area and enclosed volume. RBCs measure typically 6–8 μm in diameter and have a thickness of 2.2 μm [29]. Their average volume and surface area are 92 μm^3 and 140 μm^2, respectively [59]. Because of its biconcave shape, an RBC has 40% excess surface area compared to a sphere of the same volume, enabling the cell to undergo deformations that preserve both volume and surface area. From a mechanical point of view the RBC can be described as an incompletely inflated bag (the plasma membrane) filled with a viscous fluid (the cytoplasm) [142]. The cytoplasm behaves like a Newtonian liquid with a viscosity of approximately 6 mPa s (cP); it is mostly filled with the glycoprotein haemoglobin which is equally efficient at binding and releasing oxygen.

5.3 Mechanisms of hemolysis

The main source of haemolysis in blood pumps is the sublethal damage of the RBCs due to leaking of haemoglobin rather than catastrophic damage due to rupturing at shear rates above 42,000 s^{-1} [86]. Premature haemoglobin release shortens the RBC's normal life span

which for a healthy person is 120 days [29]. Sublethal damage does not occur immediately under stress but requires time for the RBCs to undergo deformation. The RBCs at rest aggregate into coin-stack-shaped structures called *rouleaux*, which disperse as shear stress increases. The dispersed RBCs preserve their biconcave shape and tumble in a flow with shear stress below ~ 0.1 Pa [120]. As shear increases, the tumbling slows, and the cells align with the flow at ~ 0.2 Pa. At shear stress greater than 1 Pa, they deform progressively into prolate ellipsoids with their long axes aligned parallel to the flow direction. This deformation is accompanied by an orientation of the cell in the shear planes and a rotational motion of the cell membrane around its contents [142]. Due to its resemblance with the rotation of the tread of a tank around its wheels, this phenomenon is referred to as tank-treading. If the cell is deformed by shear stresses that do not exceed a critical value and exposure time [56], it recovers its natural shape when the forces causing the deformation are removed. Even peak stress values of 1,000 Pa were found to produce only insignificant haemolysis if the exposure time did not exceed a few milliseconds [29]. The membrane can support an estimated areal strain of 6% before rupturing and has an average relaxation time depending on the membrane viscosity and elasticity which was experimentally determined as 200 ms [71]. Above 150 Pa the membrane reaches its areal strain limit, and microscopic pores in the membrane open and allow haemoglobin to leak into the blood stream. Extensive haemolysis occurs as a function of the stress and exposure time [86]. The cell membrane is to a certain extent permeable to water, oxygen, carbon dioxide and other small molecules but impermeable to haemoglobin [29]. For that reason the release of haemoglobin ΔHb into the plasma has been chosen as the indicator for haemolysis.

In order to assess quantitatively the amount of haemolysis from blood within a mock test loop, different clinical indices have been introduced; the normalized index of haemolysis (NIH) has become the American Society for Testing and Materials (ASTM) standard [5]. The NIH is related to the proportion of ΔHb and the total amount of haemoglobin Hb as

$$\mathrm{NIH}(\text{g per 100 L of blood}) = 100 \times \frac{\Delta Hb}{Hb} \times (1 - Hct) \times \kappa, \tag{5.1}$$

where Hct denotes the haematocrit (%), i.e. the proportion of blood volume occupied by RBCs (45% for a healthy person and 37% for normal bovine blood), and κ is the haemoglobin content of the blood (150 g L^{-1} for a healthy person).

5.4 Rheological modelling

In large vessels with a diameter more than two orders of magnitude greater than the size of an RBC, blood can be modelled as a homogeneous fluid [34]. At the macroscale, there exist different models with different degrees of accuracy in capturing the rheological behaviour of blood.

In CFD analysis of flow quantities inside VADs blood is usually considered as a Newtonian fluid, although it is known to display non-Newtonian properties [53, 136]. Blood's viscosity is shear-thinning because of the disaggregation of the rouleaux and the orienting of individual RBCs [40,41]. Blood also shows non-linear viscoelastic behaviour resulting from the elastic membranes of its constituents. Finally blood is thixotropic; its viscosity can vary with time at constant low shear mainly due to rouleau aggregation

and disaggregation. The viscosity of blood depends on the blood sample haematocrit and temperature, but in general the qualitative behaviour of any blood sample is the same [54]. In experimental studies [39] it has been shown that at high shear rates (above 100 s^{-1}), the viscosity of human blood with 45 % haematocrit reaches a constant value of 3.5–4.0 mPa s, thus justifying somewhat the choice of a Newtonian model for VADs.

Generalised Newtonian constitutive models, which consider shear-thinning effects, have been used to model blood, e.g. the Carreau–Yasuda model [13,63] and the modified Cross model [85]. However, complex constitutive models for blood have also been introduced, where blood is modelled as a viscoelastic fluid [7, 103, 154, 156]. In particular, constitutive equations from the Oldroyd-B class have the best potential for capturing with reasonable accuracy the rheological behaviour of blood [154, 156] while, at the same time, being tractable in complex two-dimensional and three-dimensional flows. These constitutive equations belong to the more general conformation tensor class, where the microstructure of the fluid is captured by one or more internal variables [27, 66, 68, 107, 108]. In the Oldroyd-B model, blood is assumed to consist of macromolecules (RBCs) in a Newtonian solvent (the plasma) and is accordingly modelled as a polymeric solution in which the elastic properties of a given flow are characterised by the dimensionless Weissenberg number $Wi = \lambda\dot{\gamma}$, with λ being the relaxation time of the fluid and $\dot{\gamma}$ the shear rate of the flow. Equations of the Oldroyd-B type – i.e. for viscoelastic flows – have been used recently in numerical studies of blood flow [85, 109]. The effective solution of complex flows of Oldroyd-type fluids has been an important research problem since the late 1970s [45]; recent reviews can be found in the works of Baaijens [19], Keunings [81] and Owens and Phillips [104]. A very recent review on currently used models for blood can be found in [103]. An experimental comparative study of different constitutive models for blood was conducted by Zhang [162]. Owens [103] proposes a new microstructure-based constitutive model for blood built on polymer network theory with the objective of describing rouleau aggregation and disaggregation as well as blood's shear-thinning, viscoelastic and thixotropic properties.

In the finite-element context, the solution of viscoelastic flows relies on unequal-order finite-element methods. Unequal-order finite-element methods are at a disadvantage compared to equal-order approach due to higher levels of costly indirect memory addressing on modern cache-based computer architectures.

The fact that today Newtonian modelling is generally used by the scientific community for VADs stems from its relatively good accuracy for high-shear applications and from the high computational effort involved in solving complex constitutive models for blood.

We will be modelling blood as a Newtonian fluid for the blood pump application in Sections 6 and 7. For the graft application mentioned in Section 9 in which non-Newtonian effects become important we used a shear-thinning modified Cross model. In Section 8 we describe a numerical method to solve viscoelastic flow for an Oldroyd-B fluid.

6 Flow modelling

6.1 Review of hydraulic performance prediction

Table 4 summarises previous works focussing on or including CFD-based hydraulic efficiency investigations of rotary blood pumps. Among the first numerical simulations

Table 4. *Published research in the field of hydraulic performance analysis for rotary blood pumps; AP: axial pump, CP: centrifugal pump, PVAD: pediatric VAD*

First author and year	Research team	Application	Solver
Papantonis 1988 [105,106]	Technical University of Athens, Greece	Radial pump	NA
Pinotti 1991,1995 [110,111]	Faculty of Mechanical Engineering Campinas, Brazil	Vaneless CP	SIMPLE algorithm
Bludszuweit 1995 [31]	University of Strathclyde, UK	Aries Medical Isoflow CP	CFX-TASCflow
Antaki 1995 [10] Burgreen 2001 [36] Wu 2005 [145]	McGowan Center, University of Pittsburgh, USA	Streamliner AP PediaFlow PVAD	STAR-CD
Yano 1997 [151] Ding 1998 [52] Nakamura 1999 [94]	Ohio State University, USA	IVAS CP	SMAC algorithm
Miyazoe 1999 [91]	Nikkiso Co., Ibaraki University, Japan	Nikkiso HPM-15 CP	CFX-TASCflow
Allaire 1999 [3] Anderson 2000 [9] Curtas 2002 [46] Throckmorton 2003, 2004 [134,135] Song 2004 [127] Untaroiu [138]	University of Virginia, Artificial Heart Institute, Utah, USA	HeartQuest CP, AP, PVADs	CFX-TASCflow
Ng 2000 [95] Yu 2005 [159] Chan 2002, 2005 [37,38]	Nanyang University, Singapore	MSCBP CP, AP	CFX-TASCflow, FLUENT
Qian 2000 [115] Bertram 2001 [28]	University of New South Wales, Sydney, Australia	VentrAssist CP	CFX-TASCflow
Apel 2001 [11] Arvand 2004 [16]	Helmholtz Institute, RWTH Aachen, Germany	Impella Intracardiac AP, Micro Diagonal pump	CFX-TASCflow
Watanabe 2001 [140]	Shibaura Institute of Technology, Tokyo, Japan	Biopump BP-80	CFX-TASCflow
Behr 2004 [25]	CATS, RWTH Aachen, Germany Rice University, USA	GYRO CP	XNS

to predict the hydraulic performance and shear stresses inside a blood pump were the studies performed by Papantonis and Croba [105, 106] and by Pinotti and Rosa [110, 111], who used a simplified pump model assuming an assembly of parallel co-rotating discs.

A broad variety of different blood pump applications have been analysed by the research group from the University of Utah and the University of Virginia, ranging from centrifugal [3, 9, 46, 127] and axial [138] pumps for adults to centrifugal [135] and axial [134] pumps for pediatric use.

Table 5. *Solvers and discretisation methods*

Solver	Discretisation method
SIMPLE algorithm	Finite-volume
CFX-TASCflow	Hybrid finite-volume/finite-element
STAR-CD	Finite-volume
SMAC	Finite-difference
FLUENT	Finite-volume
XNS	Finite-element

Design improvements are generally made by approaches based on the designer's intuition. The benefit of CFD in this context is that it offers the potential to guide the VAD designers towards improvements of single pump components [16, 28, 37, 46, 115].

Antaki *et al.* [10, 36, 145] have stressed the advantages of coupling between numerical simulation and mathematical optimisation techniques with the goal of an *optimal* design, which will be reviewed in Section 9.

The complex blood pump geometries have led to the common use of finite-difference methods based on overset grids or, more frequently, finite-element or volume methods based on unstructured grids. In order to solve the Navier–Stokes equations, adequate analysis tools are required in which the numerical solvers are expected to be robust and efficient. Table 5 shows which discretisation methods are used in combination with the chosen solvers. Most of the research groups listed in Table 4 have been working with the commercially available numerical solver CFX-TASCflow (before 1998 also known by the names of CFDS-Flow3D and CFX-4), which involves a hybrid finite-volume/finite-element methodology in the sense that control volumes are constructed around nodes and finite elements describe the solution variation within each element. Further commercial flow solvers for blood pump analysis that have been used in some cases are FLUENT and STAR-CD. Other research teams used their own implementations of published or self-developed algorithms; e.g. the Ohio University group listed in Table 4 used a finite-difference scheme developed by Nakamura [93] based on the simplified marker and cell (SMAC) algorithm [6]. The authors of this review have used an in-house finite-element-based code XNS in order to solve the Navier–Stokes equations of incompressible flow, employing an iterative solver generalized minimal residual method (GMRES) [118]. A decision tree and details on the authors' choice of the numerical method can be found in [22].

Results from the works cited in Table 4 show largely satisfactory agreement between hydraulic performance prediction and experimental results.

6.2 Equations governing blood flow

The isothermal, incompressible flow of a fluid in bounded domain Ω_t and boundary Γ_t is given by conservation of mass and momentum equations

$$\rho(\mathbf{u}_{,t} + \mathbf{u} \cdot \nabla\mathbf{u} - \mathbf{f}) - \nabla \cdot \boldsymbol{\sigma}(\mathbf{u}, p) = 0, \quad \text{on } \Omega_t, \tag{6.1}$$

$$\nabla \cdot \mathbf{u} = 0, \quad \text{on } \Omega_t, \tag{6.2}$$

where ρ is the fluid density (1058 kg m^{-3}); $\mathbf{u}$ is the fluid velocity and $\mathbf{u}_{,t}$ its time derivative; p is pressure; and $\mathbf{f}$ are body forces per unit mass, e.g. gravity. For a Newtonian fluid, the stress tensor $\boldsymbol{\sigma}$ is given as

$$\boldsymbol{\sigma}(\mathbf{u}, p) = -p\mathbf{I} + \mathscr{T}(\mathbf{u}), \quad \mathscr{T}(\mathbf{u}) = 2\mu\mathscr{E}(\mathbf{u}), \tag{6.3}$$

where $\mathbf{I}$ is the identity tensor; $\mathscr{T}$ is the viscous stress; μ is the viscosity (3.5 mPa s); $\mathscr{E}(\mathbf{u}) = (1/2)(\nabla\mathbf{u} + \nabla\mathbf{u}^T)$ is the rate-of-strain tensor; and $\nabla\mathbf{u}$ is the velocity gradient. The Dirichlet- and Neumann-type boundary conditions are imposed on complementary subsets $(\Gamma_t)_{\boldsymbol{g}}$ and $(\Gamma_t)_{\boldsymbol{h}}$ of the boundary Γ_t as

$$\mathbf{u} = \boldsymbol{g}, \quad \text{on } (\Gamma_t)_{\boldsymbol{g}}\ , \tag{6.4}$$

$$\mathbf{n} \cdot \boldsymbol{\sigma}(\mathbf{u}, p) = \boldsymbol{h}, \quad \text{on } (\Gamma_t)_{\boldsymbol{h}}\ . \tag{6.5}$$

6.3 Galerkin/least squares (GLS) formulation

Finite-element methods try to find an approximate solution of partial differential equations by solving a discretised form of the governing equations ((6.1) and (6.2)). Since the early 1970s the Galerkin finite-element method has been the prevailing method used in structural mechanics. However, in the context of fluid flow simulations, the Galerkin method exhibits stability problems, e.g. negative numerical diffusion which may result in spurious node-to-node oscillations in velocity for advection-dominated flow. Upwinding schemes [76], streamline–upwind/Petrov–Galerkin (SUPG) methods [35] and pressure stabilized/Petrov–Galerkin (PSPG) methods [133] were developed to overcome these shortcomings of the Galerkin method. The GLS method [77] used here combines the SUPG and PSPG stabilisations in one conceptually simple term and has proven to have good stabilisation, consistency and convergence characteristics [57, 58, 77].

In space–time methods, the stabilised finite-element formulation of the governing equations is written over the space–time domain of the problem. The finite-element function spaces are constructed by partitioning the time interval $(0, T)$ into sub-intervals $I_n = (t_n, t_{n+1})$, where t_n and t_{n+1} are arranged in a sequence of time levels $0 = t_0 < t_1 < \cdots < t_N = T$. Denoting $\Omega_n = \Omega_{t_n}$ and $\Gamma_n = \Gamma_{t_n}$, the space–time slab Q_n is defined as the domain enclosed by the surfaces Ω_n, Ω_{n+1} and P_n, with P_n being the surface formed by the boundary Γ_t as t sweeps through I_n. Analogous to Γ_t, surface P_n is decomposed into $(P_n)_{\boldsymbol{g}}$ and $(P_n)_{\boldsymbol{h}}$ with regard to the applied boundary condition (Dirichlet or Neumann). Appropriate finite-element interpolation function spaces for the velocity and pressure are then defined for space–time time slab n – $(\mathscr{S}^h_{\mathbf{u}})_n$ and $(\mathscr{S}^h_p)_n$ – as well as corresponding weighting function spaces $(\mathscr{V}^h_{\mathbf{u}})_n$ and $(\mathscr{V}^h_p)_n$. These spaces are defined as

$$(\mathscr{S}^h_{\mathbf{u}})_n = \{\mathbf{u}^h | \mathbf{u}^h \in [H^{1h}(Q_n)]^{n_{sd}},\ \mathbf{u}^h = \boldsymbol{g}^h \ on\ (P_n)_{\boldsymbol{g}}\}, \tag{6.6}$$

$$(\mathscr{V}^h_{\mathbf{u}})_n = \{\mathbf{u}^h | \mathbf{u}^h \in [H^{1h}(Q_n)]^{n_{sd}},\ \mathbf{u}^h = \mathbf{0} \ on\ (P_n)_{\boldsymbol{g}}\}, \tag{6.7}$$

$$(\mathscr{S}^h_p)_n = (\mathscr{V}^h_p)_n = \{p^h | p^h \in H^{1h}(Q_n)\}. \tag{6.8}$$

The stabilised space–time GLS formulation can be thus stated as follows: given $(\mathbf{u}^h)^-_n$, find $\mathbf{u}^h \in (\mathscr{S}^h_{\mathbf{u}})_n$ and $p^h \in (\mathscr{S}^h_p)_n$ such that $\forall \mathbf{w}^h \in (\mathscr{V}^h_{\mathbf{u}})_n$ and $\forall q^h \in (\mathscr{V}^h_p)_n$,

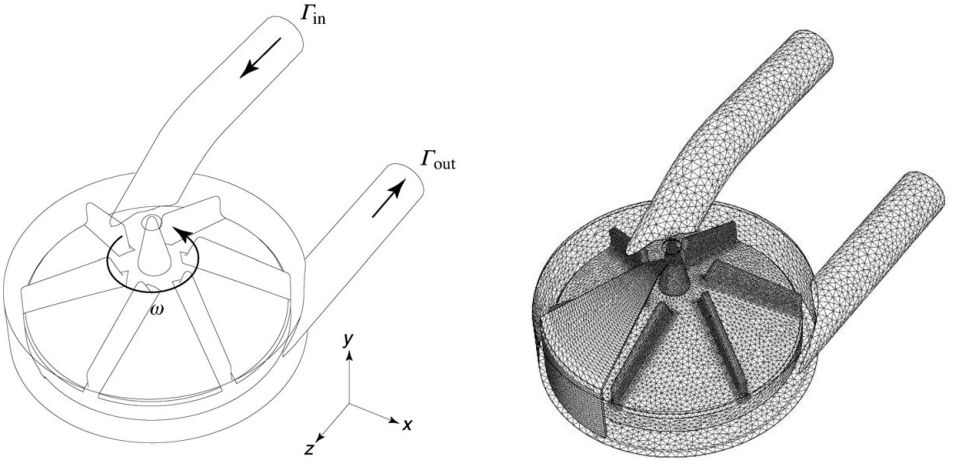

FIGURE 2. Computational domain and typical mesh for the GYRO rotary blood pump. Adapted from [25]. Copyright John Wiley & Sons. Reprinted with permission.

$$\rho\left(\mathbf{w}^h, \mathbf{u}^h_{,t} + \mathbf{u}^h \cdot \nabla \mathbf{u}^h - \mathbf{f}^h\right)_{Q_n} + (\mathscr{E}(\mathbf{w}^h), \boldsymbol{\sigma}(\mathbf{u}^h, p^h))_{Q_n} + (q^h, \nabla \cdot \mathbf{u}^h)_{Q_n}$$
$$+ \sum_{e=1}^{(n_{\text{el}})_n} \frac{\tau_{mom}}{\rho}\left(\rho\left(\mathbf{w}^h_{,t} + \mathbf{u}^h \cdot \nabla \mathbf{w}^h\right) - \nabla \cdot \boldsymbol{\sigma}(\mathbf{w}^h, q^h),\ \rho\left(\mathbf{u}^h_{,t} + \mathbf{u}^h \cdot \nabla \mathbf{u}^h - \mathbf{f}^h\right) - \nabla \cdot \boldsymbol{\sigma}(\mathbf{u}^h, p^h)\right)_{Q_n^e}$$
$$+ \rho((\mathbf{w}^h)^+_n, (\mathbf{u}^h)^+_n - (\mathbf{u}^h)^-_n)_{\Omega_n} = (\mathbf{w}^h, \boldsymbol{h}^h)_{(P_n)_{\boldsymbol{h}}}, \tag{6.9}$$

where $(\cdot,\cdot)_{\square}$ are suitable scalar or vector function inner products over domain $\square$ and $(\mathbf{u}^h)^{\pm}_n = \lim_{\varepsilon \to 0} \mathbf{u}(t_n \pm \varepsilon)$, and τ_{mom} is the stabilisation parameter – see [26] for details. The motion of the computational domain boundaries is accommodated by a deforming boundary-fitted mesh. The applied shear-slip mesh update method (SSMUM) [23] is a method that allows the elements in a thin zone of the mesh to undergo 'shear' deformation followed by limited remeshing that accommodates the desired displacement of one part of the domain with respect to another.

6.4 Experimental and numerical analysis results

The computational domain and a typical finite-element mesh for the GYRO Pump are shown in Figure 2. The inflow boundary Γ_{in} and outflow boundary Γ_{out} form the Neumann portion of the boundary ($(\Gamma_t)_{\boldsymbol{h}}$ in Section 6.3) of the boundary; the boundary conditions at the remaining surfaces are of Dirichlet type ($(\Gamma_t)_{\boldsymbol{g}}$ in Section 6.3). Experimental data is generated using a mock loop as described in [25]. Glycerol and blood are employed as test fluids, and the rotational speeds of the impeller used are $\omega = 1800$, 2000 and 2200 rpm. In the computations, appropriate pressure head can be applied between Γ_{in} and Γ_{out}. The gradual ramp-up of that pressure head leads from a strongly transient to a quasi-stationary condition of the flow field.

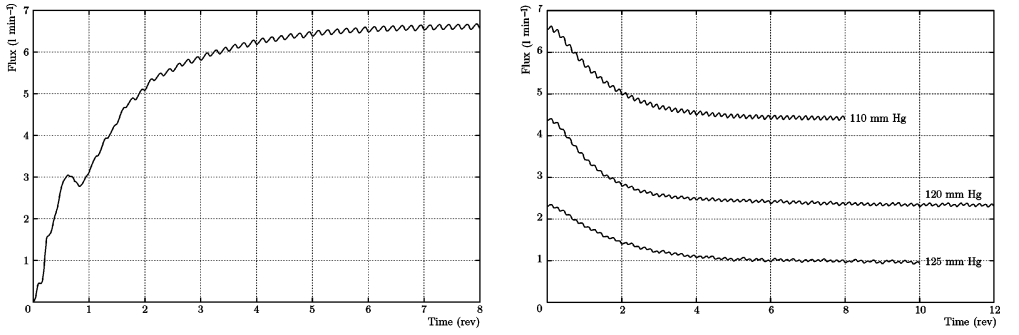

(a) $\Delta p = 100$ mm Hg (b) $\Delta p = 110$–125 mm Hg

FIGURE 3. Flux histories at Γ_{out} at $\omega = 2200$ rpm and $\Delta p = 100$, 110, 120 and 125 mmHg. Adapted from [25]. Copyright John Wiley & Sons. Reprinted with permission.

For $\omega = 2200$ rpm, the flux histories shown in Figure 3 stabilise after 6–12 revolutions of the impeller; i.e. they achieve a near-sinusoidal profile with constant average and amplitude. The simulations were performed for $\Delta p = 100$, 110, 120 and 125 mmHg with 800, 800, 1200 and 1000 time steps, respectively [25]. Flow reversal was observed at $\Delta p = 130$ mmHg.

The overall hydraulic performance at $\omega = 1800$, 2000 and 2200 rpm is presented in Figure 4. The finite range in numerical flux data is due to the low-amplitude periodic changes in the computed signal. Numerical prediction and experimental values are in good agreement for $\omega = 1800$ and 2000 rpm, while a considerable difference is observed at $\omega = 2200$ rpm, which is attributed to the limitation of the turbulence model.

All computations were performed on a Linux PC cluster, with Myrinet interconnect, on partitions ranging from 32 to 72 CPUs and requiring 4–8 hours to obtain a quasi-steady flux at each flow condition.

7 Numerical analysis of blood damage

7.1 Blood damage modelling

In spite of the intense research on blood damage modelling, there is currently no consensus on suitable models that relate fluid dynamics information, such as stress and shear rate, to clinical properties, such as the NIH.

Correlations for blood damage in artificial organs were established under the assumption of experimentally feasible conditions, which implied haemolysis under steady shear at short time intervals. Assuming that blood damage depends solely on shear stress and exposure time, several researchers have used a mathematical power-law model [65] to formulate haemoglobin release based on experimental data:

$$\frac{\Delta Hb}{Hb} = C\ \tau^a\ \Delta t^b, \tag{7.1}$$

where $\Delta Hb/Hb$ is the ratio of haemoglobin in the plasma to the total haemoglobin; τ is the scalar measure of the shear stress acting on the blood in Pa; and Δt is the

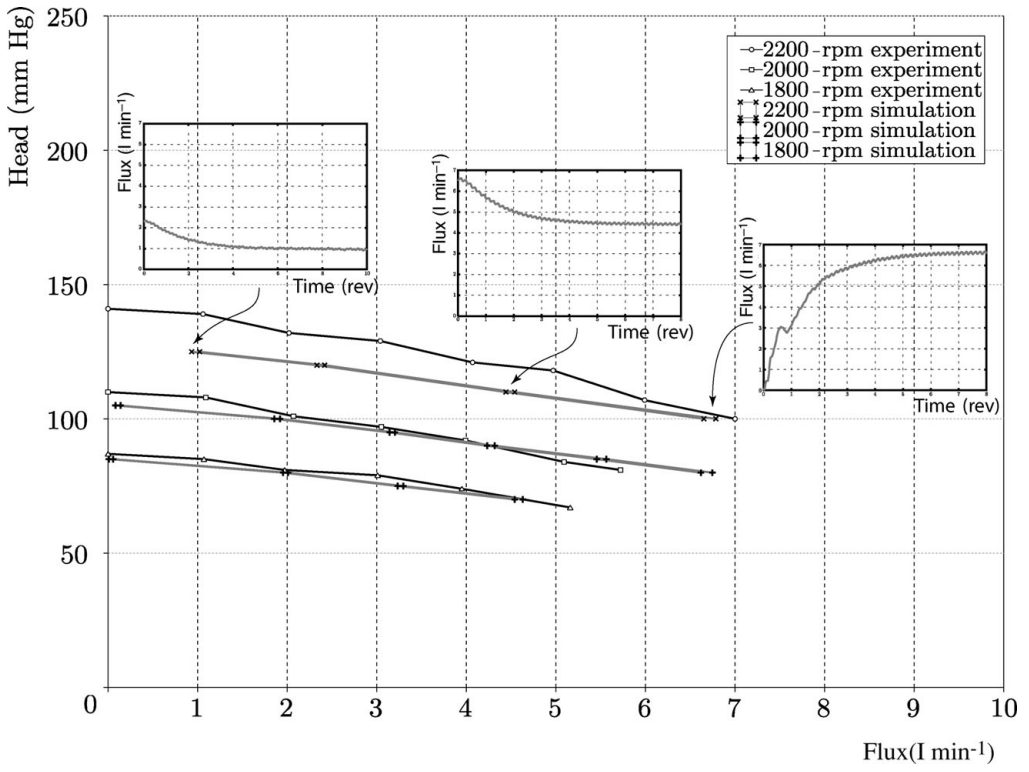

FIGURE 4. Hydraulic performance of the Gyro pump: experiment (black) versus simulation (shaded). Some of the previously shown time histories of the flux are also shown. Adapted from [25]. Copyright John Wiley & Sons. Reprinted with permission.

time duration of blood exposure to the shear stress τ in seconds. Gu and Smith [67] used a benchmark approach for an evaluation of different existing models presented by Giersiepen *et al.* [62], Heuser and Opitz [73] and Grigioni *et al.* [65] to evaluate the blood damage prediction accuracy of such models compared to experimental data. For haematological CFD design of VADs, the most commonly adopted model considering steady-shear haemolysis experiments is the one established by Giersiepen *et al.* [62] who derived the constants C, a and b from an empirical study in a cylindrical Couette system undertaken by Wurzinger *et al*. [147]. The following correlation was found:

$$\frac{\Delta Hb}{Hb} = 3.62 \times 10^{-7}\, \tau^{2.416}\, \Delta t^{0.785}. \tag{7.2}$$

Further studies in a modified Couette system including measurements for time-varying shear stress were performed by Klaus [82], who uses an improved sealing system to exclude effects of temperature-induced haemolysis. Different authors have applied comparative stress theory to compute the scalar measure of τ in equation (7.1) from the second invariant of the deviatoric stress tensor:

$$\tau = (-II_{\mathscr{T}})^{\frac{1}{2}} = \left(\frac{1}{2}\mathscr{T} : \mathscr{T}\right)^{\frac{1}{2}}. \tag{7.3}$$

In the following, this method of computing haemolysis will be referred to as stress-based method; it assumes that the RBC's response to load is immediate and independent of its load history. Bludszuweit [31] expressed the scalar shear stress value based on the von Mises criterion [79] which is calculated from the six components of the stress tensor:

$$\tau = \left(\frac{1}{6}((\sigma_{xx} - \sigma_{yy})^2 + (\sigma_{yy} - \sigma_{zz})^2 + (\sigma_{zz} - \sigma_{xx})^2) + \left(\sigma_{xy}^2 + \sigma_{yz}^2 + \sigma_{zx}^2\right)\right)^{\frac{1}{2}}. \tag{7.4}$$

Since then, this approach has been further elaborated to include some aspects of stress threshold and aging, as well as calibration for a specific device [16, 64, 155].

In contrast to the stress-based method, the authors' group presented a strain-based approach which will be described in Section 7.3.

7.2 Evaluation of hemolysis simulations

Equation (7.4) was introduced to assign scalar stress values to pathlines, where each of them represents a particle's path through the blood pump chamber. Based on this approach, Bludszuweit [32] described the methodology on how CFD can be used for haemolysis predictions in artificial organs and calculated overall damage as the sum of the partial influences of the loading function assuming constant and cyclic load functions to reflect RBCs' damage behaviour or resistance. In [30]–[32], the stress-loading time functions for individual particles are determined for the Aries Medical Isoflow centrifugal blood pump and other types of artificial organs.

Between 1995 and 2001 other researchers began to use CFD in order to find a good haematological design for centrifugal blood pumps [88, 159], axial blood pumps [12] or simplified blood pump models [111, 153] by relating local flow conditions to haemolysis. In those studies, haemolysis was discussed, but blood damage was not quantified. In absence of quantitative haemolysis results, some authors interpreted peak stresses as threshhold levels for the occurence of haemolysis [159].

By comparison to experimental data, it was found that equation (7.2) tends to overestimate the actual blood damage in artificial organs. To cite some examples, De Wachter and Verdonck [50] found the computed haemolysis values for cannulae to lie in a range that was 2 to 8 times the measured values; Goubergrits and Affeld [64] found a computed overestimation factor of 25 for a standard Björk-Shiley valve; and Yano *et al.* [152] found a factor of 30 for the case of an axial blood pump; in all these cases, a stress-based approach was used. Grigioni *et al.* [65] drew attention to the inherent limitations of haemolysis estimations based on power laws such as the one proposed by Giersiepen *et al.* [62] and highlighted the effect of a time-varying loading acting on RBCs, showing the need for a reassessment of the power-law model or, more precisely, the interpretation of the stress measure used in that model.

More recently, quantitative haematological CFD results based on a stress-based model and considering blood as a Newtonian fluid have been published for rotary blood pump designs [16, 17, 37, 90, 124, 127, 161] and for pulsatile blood pumps [100]. These authors used either Giersiepen's power-law equation (7.2) or Bludszuweit's stress model equation (7.4) – or both. For the above-mentioned rotary blood pump simulations, TASCflow was typically

chosen as the solver, and a Lagrangian particle tracking method was applied to add up the haemoglobin leakages along streamlines. Some novel approaches and insights regarding haemolysis predictions have been introduced:

Comparative studies

Mitoh *et al.* [90], Song *et al.* [124,127] and Zhang *et al.* [161] reported good agreement of CFD blood damage predictions with experimental haemolysis data, thus demonstrating that CFD is a viable approach to analyse blood behaviour in a VAD.

Choice of best design alternative

Arvand *et al.* [16] and Chan *et al.* [37] undertook their studies with the objective of finding the best haematological design for individual blood pump components from a predetermined set of different design options by comparing the computed blood damage rates for the competing design candidates.

Semi-empirical pump-specific haemolysis model

Arvand *et al.* [17] set the estimated haemolysis index equal to the measured index and determined the constants of the power law by regression analysis in order to receive the best fit. This results in an optimised haemolysis model, albeit restricted to a single pump configuration.

Shape optimisation

Wu *et al.* [145] proposed a parameterised geometry model of the blood pump and demonstrated an automatical optimisation design approach; this topic is further discussed in Section 9.

Influence of turbulence

Some researchers have stressed the important role of turbulence. Kameneva *et al.* [80] performed experiments in combination with CFD studies and found significantly varying haemolysis values at constant shear stress values for turbulent compared to laminar flow. In a comparative study between PIV and CFD-based analysis, Song *et al.* [126] found that the accuracy of flow predictions depends on the applied turbulence model, especially in near-wall regions.

Influence of device orientation

Yuri *et al.* [160] found that the implantation position and orientation of the blood pump in the patient can have an influence on haemolysis. This is especially the case for the GYRO pump in which implantation orientation affects the location of the magnetically levitated impeller.

7.3 Modelling of RBC strain

As an alternative to stress-based models our research team has recently proposed a more fundamental approach [14] that takes into account the time-dependent history of RBC deformation, which may not correspond to the instantaneous shear stress levels in the surrounding fluid. This approach requires a mathematical representation of the RBC geometry.

In the scientific literature models of RBC deformation can be found in works focussing on microscale blood flow in which RBCs are usually modelled as capsules [148]. A capsule is a particle with an elastic membrane enclosing a fluid. A description of the modelling and simulation of capsules can be found in [112, 113]. Applications of this approach to RBCs include simulation of simple shear flow [55, 114], capillary flow [122] and rouleau aggregation [20]. It was observed that RBCs in shear flow behave as liquid droplets [60, 120]. In droplets, as opposed to capsules, the interfacial forces arise from surface tension. Microcapsules and biological cells such as RBCs represent an intermediate case between elastic solid particles and liquid droplets, behaving rather as a solid-like body in the low-shear regime and attaining a steady-state orientation with a tank-treading motion of the membrane only at high shear rates [21, 123].

Therefore in blood pumps in which shear forces are typically high, our research group uses the simplified model of RBCs as neutrally buoyant droplets. Other authors have also used a droplet analogy to simulate RBC flow behaviour in small and intermediate vessels [43, 44, 121].

In our model the RBC shape is described by an evolution equation that incorporates specific characteristics of RBCs including shape recovery in the absence of shear and tank-treading motion. The RBC shape is simply described by a symmetric positive-definite morphology tensor, which is subject to deformations due to forces exerted by the surrounding liquid. These forces compete with the interfacial tension, which tends to reduce the elongation of the ellipsoid, which can be modelled as spherical-shaped restoration force (at high shear). A frame-invariant droplet deformation equation was proposed by Maffetone and Minale [87], which accounts for non-affine droplet deformation, and extended by Arora *et al.* [14] to represent tank-treading:

$$\frac{\mathrm{d}\mathscr{B}}{\mathrm{d}t} - [\boldsymbol{\Omega}\cdot\mathscr{B} - \mathscr{B}\cdot\boldsymbol{\Omega}] = -f_1[\mathscr{B} - g(\mathscr{B})\mathscr{I}] + f_2[\widetilde{\mathscr{E}}\cdot\mathscr{B} + \mathscr{B}\cdot\widetilde{\mathscr{E}}] + f_3[\widetilde{\mathscr{W}}\cdot\mathscr{B} - \mathscr{B}\cdot\widetilde{\mathscr{W}}], \tag{7.5}$$

where $\mathscr{B}$ is the morphology tensor; $\mathscr{W} = (1/2)(\nabla\mathbf{u} - \nabla\mathbf{u}^T)$ is the vorticity tensor; $g(\mathscr{B}) = 3\,III/II$ (involving third and second invariants of $\mathscr{B}$); $f_1 = 5.0\ \mathrm{s}^{-1}$ based on RBC relaxation time; and $f_2 = f_3 = 1.25 \times 10^{-3}$ are uniquely determined by RBC behaviour in steady shear flow. The orthonormal matrix $\boldsymbol{\Omega}$ defines the rate of rotation of a reference frame attached to the eigenvectors of $\mathscr{B}$, leading to $\widetilde{\mathscr{E}} = \mathscr{E}$ and $\widetilde{\mathscr{W}} = \mathscr{W} - \boldsymbol{\Omega}$. At any instant, the flow field is simulated, and the morphology tensor evolution is tracked along pathlines through the pump. In this way, equation (7.5) yields information about the deformation, or strain, of the RBC at each point in the flow field. Because RBCs experiencing varying shear stresses require time to change their shape, the calculated

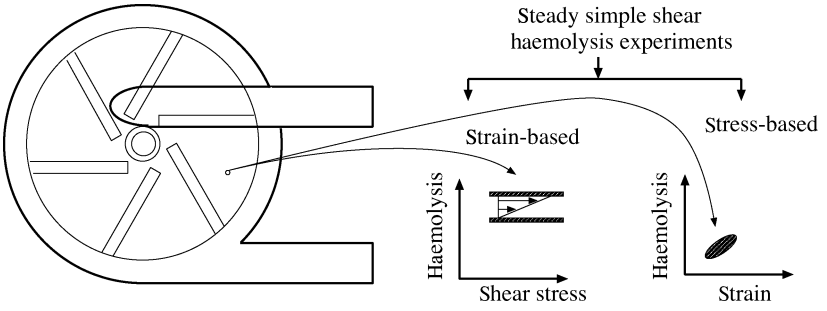

FIGURE 5. Stress- and strain-based haemolysis predictions for the centrifugal blood pump. Adapted from [15]. Copyright Blackwell Publishing. Reprinted with permission.

strain acting on the blood cell does not lead to an instantaneous deformation as in the way predicted by steady-shear experiments. Therefore, the computed deformation of the RBC is correlated to a hypothetical shear that would lead to such deformation under steady conditions. Based on these shear values, the haemolysis rate can be computed using the experimental correlation given by the equation (7.2). Next, the haemolysis rate is integrated along each pathline to calculate blood damage for individual RBCs, and by taking the average over a sufficiently high number of pathlines, it is possible to calculate the haemoglobin release in the blood pump; this approach is referred to as the strain-based model [14].

Figure 5 schematically shows the difference between the stress- and strain-based modelling approaches.

8 Viscoelastic modelling of blood

The authors have been developing GLS-type finite-element methods for solving the flow of viscoelastic fluids [22,24,42]; the most recent version is the GLS4 method [42], where the equations of the flow are converted into a set of first-order partial differential equations, and the four flow field variables (velocity, pressure, velocity gradient and elastic stress) are represented explicitly by basis functions – hence the name GLS4. This method is outlined below as an example of the mathematical complexity needed to handle viscoelastic flow equations.

The GLS4 method is attractive for large-scale computations, e.g. flow in a complicated three-dimensional blood pump. One characteristic of the GLS4 method is the use of low- and equal-order interpolation functions for all variables, which makes the method efficient and easy to implement on distributed-memory clusters.

In addition to the conservation of momentum and mass equations (6.1) and (6.2), the traceless velocity gradient and the transport of conformation are considered; the traceless velocity gradient $\mathbf{L}$ is defined as

$$\mathbf{L} = \nabla\mathbf{u} - \frac{1}{\mathrm{tr}\,\mathbf{I}}(\nabla \cdot \mathbf{u})\,\mathbf{I}, \tag{8.1}$$

where tr denotes trace, while the conformation tensor $\mathbf{M}$ for the Oldroyd-B model obeys the evolution equation:

$$Wi\ (\mathbf{u}\cdot\nabla\mathbf{M}-\mathbf{L}^T\cdot\mathbf{M}-\mathbf{M}\cdot\mathbf{L})+(\mathbf{M}-\mathbf{I})=\mathbf{0}, \tag{8.2}$$

where the non-dimensional Weissenberg number Wi represents the product of the relaxation time and the shear rate of the flow.

Equation (6.3), for the Oldroyd-B model, expands to

$$\boldsymbol{\sigma}=-p\mathbf{I}+\mathscr{T}_1+\mathscr{T}_2,\quad \mathscr{T}_1=\mu_s(\mathbf{L}+\mathbf{L}^T),\quad \mathscr{T}_2=\frac{\mu_p}{\lambda}\ (\mathbf{M}-\mathbf{I}), \tag{8.3}$$

where $\boldsymbol{\sigma}$ is the stress tensor; $\mathscr{T}_1$ is the viscous stress; $\mathscr{T}_2$ is the elastic contribution to the stress; μ_s is the solvent viscosity; μ_p is the polymer contribution to the viscosity; and λ is the relaxation time of the viscoelastic fluid. The GLS4 formulation for steady flow of an inertialess incompressible viscoelastic fluid occupying a spatial domain Ω is as follows: Find $\mathbf{u}^h\in\mathscr{S}^h_{\mathbf{u}}$, $p^h\in\mathscr{S}^h_p$, $\mathbf{L}^h\in\mathscr{S}^h_{\mathbf{L}}$ and $\mathbf{M}^h\in\mathscr{S}^h_{\mathbf{M}}$ such that

$$\begin{aligned}
&\int_\Omega \nabla\mathbf{w}^h:\boldsymbol{\sigma}^h\mathrm{d}\Omega+\int_{\Gamma_h}\mathbf{w}^h\cdot\mathbf{h}^h\mathrm{d}\Gamma\\
&\quad+\int_\Omega \tau_{mom}\left[\nabla q^h-\beta\nabla\cdot(\mathbf{E}^h+(\mathbf{E}^h)^T)-\frac{(1-\beta)}{Wi}\nabla\cdot\mathbf{S}^h\right]\cdot[-\nabla\cdot\boldsymbol{\sigma}^h]\mathrm{d}\Omega\\
&\quad+\int_\Omega q^h(\nabla\cdot\mathbf{u}^h)\mathrm{d}\Omega\\
&\quad+\int_\Omega \tau_{cont}(\nabla\cdot\mathbf{w}^h)(\nabla\cdot\mathbf{u}^h)\mathrm{d}\Omega\\
&\quad+\int_\Omega \mathbf{E}^h:\left[\mathbf{L}^h-\nabla\mathbf{u}^h+\frac{1}{\mathrm{tr}\ \mathbf{I}}(\nabla\cdot\mathbf{u}^h)\mathbf{I}\right]\mathrm{d}\Omega\\
&\quad+\int_\Omega \tau_{gradu}\left[\mathbf{E}^h-\nabla\mathbf{w}^h+\frac{1}{\mathrm{tr}\ \mathbf{I}}(\nabla\cdot\mathbf{w}^h)\mathbf{I}\right]:\left[\mathbf{L}^h-\nabla\mathbf{u}^h+\frac{1}{\mathrm{tr}\ \mathbf{I}}(\nabla\cdot\mathbf{u}^h)\mathbf{I}\right]\mathrm{d}\Omega\\
&\quad+\int_\Omega \mathbf{S}^h:[Wi(\mathbf{u}^h\cdot\nabla\mathbf{M}^h-(\mathbf{L}^h)^T\cdot\mathbf{M}^h-\mathbf{M}^h\cdot\mathbf{L}^h)+(\mathbf{M}^h-\mathbf{I})]\mathrm{d}\Omega\\
&\quad+\int_\Omega \tau_{cons}[Wi\ (\mathbf{u}^h\cdot\nabla\mathbf{S}^h-(\mathbf{L}^h)^T\cdot\mathbf{S}^h-\mathbf{S}^h\cdot\mathbf{L}^h)+\mathbf{S}^h]:\\
&[Wi\ (\mathbf{u}^h\cdot\nabla\mathbf{M}^h-(\mathbf{L}^h)^T\cdot\mathbf{M}^h-\mathbf{M}^h\cdot\mathbf{L}^h)+(\mathbf{M}^h-\mathbf{I})]\mathrm{d}\Omega\ =\ 0,\\
&\qquad\forall q^h\in\mathscr{V}^h_p,\ \forall\mathbf{w}^h\in\mathscr{V}^h_{\mathbf{u}},\ \forall\mathbf{E}^h\in\mathscr{V}^h_{\mathbf{L}},\ \forall\mathbf{S}^h\in\mathscr{V}^h_{\mathbf{M}},
\end{aligned} \tag{8.4}$$

where $\beta=\mu_s/(\mu_s+\mu_p)$ is the viscosity ratio; $\mathscr{S}^h$ and $\mathscr{V}^h$ are suitably defined interpolation and weighting function spaces for the velocity, pressure, velocity gradient and conformation; and $\tau_{mom},\tau_{cont},\tau_{gradv}$ and τ_{cons} are the least squares stabilisation parameters for the momentum, continuity, interpolated traceless velocity gradient and constitutive equations, defined as

$$\tau_{mom}=\frac{h^2}{4},\quad \tau_{cont}=0,\quad \tau_{gradv}=1, \tag{8.5}$$

$$\tau_{cons}=\left[1+(Wi\,\|\mathbf{L}^h\|)^2+\left(\frac{2Wi\,\|\mathbf{u}^h\|}{h}\right)^2\right]^{-1/2}, \tag{8.6}$$

where h is the dimensionless element length. This formulation has been applied to a benchmark problem of an Oldroyd-B fluid past a circular cylinder in a channel with a width that is two times the cylinder diameter [42], where good agreement with the published results [78, 129] was found. The GLS4 method may be of course extended to unsteady flows; however, such extension has not been yet tested.

9 Design optimization

In the context of blood pump development, considerable research on CFD-based *design optimisation* has been made by Antaki *et al.* [10], Burgreen *et al.* [36] and Wu *et al.* [145]. The expression *design optimisation* does not admit a universally accepted interpretation and is often confounded with the term *design improvement*. *Design optimisation* denotes an automated iterative improvement process, in which numerical simulation is coupled with optimisation techniques. This fully automated procedure stands in marked contrast to a design approach including a human expert in the iteration loop. The *design optimisation* process is an iterative approach which has been described in [10, 36] and consists in the following steps:

- an initial shape of the device is defined;
- geometrical features which are chosen to be variable are parametrised;
- objective functions are defined resulting in a specified performance index;
- CFD simulations are performed to characterise the flow field in terms of fluid dynamics properties;
- the objective function and its gradient are computed or estimated and analysed with respect to their optimality;
- as long as the performance index is sub-optimal the shape parameters are modified, and an additional iteration is performed.

Requirements and specific aspects for design optimisation compared to design improvement are listed in Table 6.

The *design optimisation* strategy for blood pumps was first presented by Antaki *et al.* [10], but many obstacles made its application a difficult task. According to Antaki *et al.* [10], the main challenges lie in finding enhanced models for the description of the blood flow, a better description of the relationship between macroscopic and microscopic blood flow features and adequate automated algorithms for performing shape changes in response to computed flow features.

Design optimisation is a systematic methodology. For the iterations, neither heuristic knowledge nor human interaction is required, and cut-and-try approaches are avoided. As the complexity of the problem rises, it becomes an increasingly time-saving and efficient method leading to an optimal solution. A particularly strong benefit of *design optimisation* is the possibility of reaching an optimal compromise between competing design objectives by means of defining a corresponding performance index.

Wu *et al.* [145] presented results from CFD-based design optimisation for the improvement of flow characteristics of a blood pump impeller. In this case blood was assumed to be Newtonian.

Table 6. *Features and requirements of design optimisation and design improvement*

	Design optimisation	Design improvement
Blood pump model	Complex parametric geometry model required	Simple non-parametric geometry model sufficient
Blood flow model	Enhanced model required	Enhanced model desirable
Computational effort	Computation of flow field and its derivatives for shape changes, many iterations	Computation of flow field, few iterations
Solver	Efficient solver required	Efficient solver required
Computational cost	Very high	High
Mesh adaptation	Automated	Manual
Degree of automation	Fully automated approach, limited human interaction required	Heuristic knowledge and human interaction required
Competing design criteria	Optimal compromise between competing design criteria can be found by defining objective functions and a corresponding performance index	Competing design objectives add difficulties in finding best compromise
Obtainable result	Optimal result, can solve highly complex cases, optimal solution can be found outside the scope of human intuition	Can find best solution in a set of intuition-based alternatives

The authors' group has also successfully applied design optimisation for steady [1] and unsteady [2] blood flows. These study cases include arterial grafts and are less complex than a blood pump as far as geometry is concerned; however, additional complexity was introduced by modelling blood as a shear-thinning fluid.

In our study the goal was to find a shape $\Omega(\boldsymbol{\alpha})$ for the graft such that a given objective function J, which depends on the design variable $\boldsymbol{\alpha}$, is minimised. The Navier–Stokes equations (6.1) and (6.2) are written as a generic state equation:

$$\mathbf{c}(\mathbf{u}, p; \mathbf{x}) = 0. \tag{9.1}$$

The set of admissible shapes can be parameterised by $\boldsymbol{\alpha} \in \mathscr{A}_{ad} \subset \mathbb{R}^n$, so that the optimal design problem is given as follows:

$$\text{minimise} \quad J(\boldsymbol{\alpha}), \tag{9.2}$$

$$\text{subject to} \quad \mathbf{c}(\mathbf{u}(\boldsymbol{\alpha}), p(\boldsymbol{\alpha}); \mathbf{x}(\boldsymbol{\alpha})) \text{ with } \Omega = \Omega(\boldsymbol{\alpha}), \tag{9.3}$$

$$\boldsymbol{\alpha} \in \mathscr{A}_{ad}. \tag{9.4}$$

In order to avoid high-shear regions in the graft the objective function is chosen as the integral of the squared shear rate over the observation region $\Omega_{\mathsf{obs}}(\boldsymbol{\alpha}) \subset \Omega(\boldsymbol{\alpha})$,

$$J(\boldsymbol{\alpha}) = 2 \int_{\Omega_{\mathsf{obs}}(\boldsymbol{\alpha})} \mathscr{E}(\mathbf{u}) : \mathscr{E}(\mathbf{u}) \mathrm{d}\mathbf{x}. \tag{9.5}$$

The discrete state equation is written as

$$\mathbf{c}^h(\mathbf{v}^h(\boldsymbol{\alpha}), \mathbf{x}^h(\boldsymbol{\alpha})) = 0, \tag{9.6}$$

where $\mathbf{v}^h = (\mathbf{u}^h, p^h)$. The discrete counterpart of the optimisation problem can be written as

$$\text{minimise } \widehat{J}^h(\boldsymbol{\alpha}), \tag{9.7}$$

$$\text{subject to } \boldsymbol{\alpha} \in \mathscr{A}_{ad}, \tag{9.8}$$

where $\widehat{J}^h(\boldsymbol{\alpha}) = J^h(\mathbf{v}^h(\boldsymbol{\alpha}), \mathbf{x}^h(\boldsymbol{\alpha}), \boldsymbol{\alpha})$. We use a gradient-based algorithm to solve the problem, where the gradient of $\widehat{J}^h$ with respect to $\boldsymbol{\alpha}$ is given by

$$\nabla \widehat{J}^h = \frac{\partial J^h}{\partial \boldsymbol{\alpha}} + \frac{\partial J^h}{\partial \mathbf{x}^h} \frac{\mathrm{d}\mathbf{x}^h}{\mathrm{d}\boldsymbol{\alpha}} + \frac{\partial J^h}{\partial \mathbf{v}^h} \frac{\mathrm{d}\mathbf{v}^h}{\mathrm{d}\boldsymbol{\alpha}}. \tag{9.9}$$

By computing $\delta\boldsymbol{\alpha}$ the new $\boldsymbol{\alpha} = \boldsymbol{\alpha} + \delta\boldsymbol{\alpha}$ can be determined, and the mesh $\mathbf{x}^h(\boldsymbol{\alpha})$ is updated for the next iteration.

As a result of the performed analysis, it became clear that the optimal shape can show striking discrepancies in terms of fluid dynamic parameters for optimisation results based on different constitutive models.

10 Conclusion

We have presented a review of current VAD designs, described their design requirements and outlined the important role of CFD in the context of VAD development.

We have then reviewed current understanding of the complex structure of blood, including its shear-thinning and viscoelastic behaviour, as well as tank-treading of RBCs.

We have further presented an overview of published research and current state-of-the-art methods for the analysis of blood flow processes in VADs. Details on numerical computations performed by our research team including quantitative results for unsteady blood flow have been given for the GYRO blood pump. We have shown that CFD-based predictions of hydraulic pump performance fit well the experimental data at lower rotational speeds. It is expected that the implementation of a more accurate turbulence model will be able to achieve better agreement for higher impeller rotational speeds.

Most of the works reviewed in this paper assume blood behaves like a Newtonian fluid and reduce the three-dimensional shear forces acting on the RBCs by a scalar shear-stress value, which is then correlated to experimental results under steady flow. We called this method stress-based, as it assumes immediate response of RBCs to instantaneous stress values.

We have pointed out that predicting mechanical haemolysis in a blood pump is a more complex task and requires realistic haemorheological and blood damage models.

To that end, our research team has developed a tensor RBC model, derived from a model of a deforming droplet and modified to include tank-treading. By computing the morphological change of the RBCs along their pathlines through the pump, it is

possible to determine haemolysis based on the RBC deformation; we called this approach a strain-based method.

We have reviewed viscoelastic modelling of blood with the Oldroyd-B model. The GLS4 method for solving steady flow of viscoelastic fluids has been reviewed, which is easy to implement, as it uses equal-order polynomial interpolations for all variables. Our research team is working on the development of the unsteady GLS4 method to simulate the flow through blood pumps.

The advances of design optimisation in the field of VAD development have been reviewed, and it was concluded that, whereas the optimisation strategy has already been well described in its theory, it has not yet been applied for a complex parameterised blood pump model. Demanding implementation and computational requirements have made its application difficult. However, we have discussed the advantages of design optimisation compared to a mere design improvement strategy and believe that design optimisation has a powerful potential.

Future research will be directed towards further elaboration of blood and haemolysis models. The implementation of adequate turbulence models becomes important especially at high rotational speeds. The development of a thrombosis model, although not discussed in detail in this paper, will be of importance in order to treat the subject of blood damage in a holistic manner. Comparative studies in blood pumps between a stress-based and a strain-based method for calculating haemolysis will serve to evaluate the predictive potential of these methods. Possibilities to further increase the performance of the GLS4 method, as specified in [42], are also being considered.

In the context of design optimisation the research for realistic constitutive blood models will be of particular importance, as different results may be obtained depending on the constitutive model.

Acknowledgements

This work was supported by the National Science Foundation under the award CTS-ITR-0312764, by the MicroMed company, by the German Science Foundation under the GSC 111, SFB 401, SFB 540, SPP1253 and SPP 1273 programmes and by JARA Seed funds. Computing resources were provided by the RWTH Aachen University Center for Computing and Communication and by the Forschungszentrum Jülich. Additional computing resources were provided by the Rice CRAY XD1 Cluster, funded by the NSF through an MRI award CNS-0421109, Rice University, AMD and CRAY and were also provided by the Rice Terascale Cluster funded by the NSF under grant EIA-0216467, Intel and Hewlett-Packard. Further research in the field is supported by NIH grant 1R01HL085054-01A2 through the Texas Heart Institute. We wish to thank Mr Bob Benkowski from MicroMed for his strong support.

References

[1] Abraham, F., Behr, M. & Heinkenschloss, M. (2005) Shape optimization in steady blood flow: A numerical study of non-Newtonian effects. *Comp. Meth. Biomech. Biomed. Eng.* **8**(2), 127–137.

[2] Abraham, F., Behr, M. & Heinkenschloss, M. (2005) Shape optimization in unsteady blood flow: A numerical study of non-Newtonian effects. *Comp. Meth. Biomech. Biomed. Eng.* **8**(3), 201–212.

[3] Allaire, P. E., Wood, H. G., Awad, R. S. & Olsen, D. B. (1999) Blood flow in a continuous flow ventricular assist device. *Artif. Organs* **23**(8), 769–773.

[4] The American Heart Association. (2006) Heart disease and stroke statistics: 2006. *Circulation* **113**, 85–151.

[5] American Society for Testing and Materials. (1997) Standard practice for assessment of hemolysis in continuous flow blood pumps. Standard F 1841-97, ASTM.

[6] Amsden, A. A. & Harlow, F. H. (1970) *The SMAC method: A numerical technique for calculating incompressible fluid flows. Technical Report LA-4370,* Los Alamos Scientific Lab., New Mexico.

[7] Anand, M. & Rajagopal, K. R. (2004) A shear-thinning fluid model for describing the flow of blood. *Int. J. Cardiovasc. Med. Sci.* **4**(2), 59–68.

[8] Anderson, D. W. (2001) Blood pumps: Technologies and markets in transformation. *Artif. Organs* **25**(5), 406–410.

[9] Anderson, J. B., Wood, H. G., Allaire, P. E., Bearnson, G. & Khanwilkar, P. (2000) Computational flow study of the continuous flow ventricular assist device, prototype number 3 blood pump. *Artif. Organs* **24**(5), 377–385.

[10] Antaki, J. F., Ghattas, O., Burgreen, G. W. & He, B. (1995) Computational flow optimization of rotary blood pump components. *Artif. Organs* **19**(7), 608–615.

[11] Apel, J., Neudel, F. & Reul, H. (2001) Computational fluid dynamics and experimental validation of a microaxial blood pump. *ASAIO* **47**, 552–558.

[12] Apel, J., Paul, R., Klaus, S., Siess, T. & Reul, H. (2001) Assessment of hemolysis related quantities in a microaxial blood pump by computational fluid dynamics. *Artif. Organs* **25**(5), 341–347.

[13] Arora, D. (2005) *Computational Hemodynamics: Hemolysis and Viscoelasticity. PhD thesis,* Department of Mechanical Engineering and Materials Science, Rice University, Houston, TX.

[14] Arora, D., Behr, M. & Pasquali, M. (2004) A tensor-based measure for estimating blood damage. *Artif. Organs* 28(11), 1002–1015.

[15] Arora, D., Behr, M. & Pasquali, M. (2006) Hemolysis estimation in a centrifugal blood pump using a tensor-based measure. *Artif. Organs* **30**, 539–547.

[16] Arvand, A., Hahn, N., Hormes, M., Akdis, M., Martin, M. & Reul, H. (2004) Comparison of hydraulic and hemolytic properties of different impeller designs of an implantable rotary blood pump by computational fluid dynamics. *Artif. Organs* **28**(10), 892–898.

[17] Arvand, A., Hormes, M. & Reul, H. (2005) A validated computational fluid dynamics model to estimate hemolysis in a rotary blood pump. *Artif. Organs* **29**(7), 531–540.

[18] Avrahami, I., Einav, S., Rosenfeld, M. & Affeld, K. (2001) Hemodynamic aspects of the Berlin ventricle assist device. In*: Proceedings of the 23rd Annual EMBS International Conference*, October 25–28, IEEE Press: Istanbul, Turkey, pp. 468–472.

[19] Baaijens, F. P. T. (1998) Mixed finite element methods for viscoelastic flow analysis: A review. *J. Non-Newton. Fluid Mech.* **79**, 361–385.

[20] Bagchi, P., Johnson, P. C. & Popel, A. S. (2005) Computational fluid dynamic simulation of aggregation of deformable cells in a shear flow. *J. Biomech. Eng.* **127**, 1070–1080.

[21] Barthès-Biesel, D. & Sgaier, H. (1985) Role of membrane viscosity in the orientation and deformation of a spherical capsule suspended in shear flows. *J. Fluid Mech.* **160**, 119–135.

[22] Behr, M. (1992) *Stabilized Finite Element Methods for Incompressible Flows With Emphasis on Moving Boundaries and Interfaces. PhD thesis,* Department of Aerospace Engineering and Mechanics, University of Minnesota, Minneapolis, MN.

[23] Behr, M. & Arora, D. (2003) Shear-slip mesh update method: Implementation and applications. *Comp. Meth. Biomech. Biomed. Eng.* **6**(2), 113–123.

[24] Behr, M., Arora, D., Coronado, O. & Pasquali, M. (2005) GLS-type finite element methods for viscoelastic fluid flow simulation. In: K. J. Bathe (editor), *Proceedings of the Third MIT Conference on Computational Fluid and Solid Mechanics*, Elsevier Science Ltd., Camebridge, MA, pp. 586–589.

[25] Behr, M., Arora, D., Nosé, Y. & Motomura, T. (2004) Performance analysis of ventricular assist devices using finite element flow simulation. *Int. J. Numer. Meth. Fluids* **46**, 1201–1210.

[26] Behr, M. & Tezduyar, T. E. (1994) Finite element solution strategies for large-scale flow simulations. *Comp. Meth. Appl. Mech. Eng.* **112**, 3–24.

[27] Beris, A. N. & Edwards, B. J. (1994) *Thermodynamics of Flowing Systems With Internal Microstructure*, 1st edn., Oxford University Press, Oxford.

[28] Bertram, C. D., Qian, Y. & Reizes, J. A. (2001) Computational fluid dynamics performance prediction of the hydrodynamic bearings of the VentrAssist rotary blood pump. *Artif. Organs* **25**(5), 348–357.

[29] Blackshear, P. L. & Blackshear, G. L. (1987) Mechanical hemolysis. In: R. Skalak & S. Chien (editors), *Handbook of Bioengineering*, McGraw-Hill, New York, pp. 15.1–15.19.

[30] Bludszuweit, C. (1995) Model for a general mechanical blood damage prediction. *Artif. Organs* **19**(7), 583–589.

[31] Bludszuweit, C. (1995) Three-dimensional numerical prediction of stress loading of blood particles in a centrifugal pump. *Artif. Organs* **19**(7), 590–596.

[32] Bludszuweit, C. (1997) Evaluation and optimization of artificial organs by computational fluid dynamics. In: *Proceedings of 1997 ASME Fluids Engineering Division Summer Meeting*. Vancouver, British Columbia, Canada, ASME. June 22–26, 1997.

[33] Blümich, B. (2005) *Essential NMR*. Springer, Berlin.

[34] Boryczko, K., Dzwinel, W. & Yuen, D. A. (2003) Dynamical clustering of red blood cells in capillary vessels. *J. Mol. Model.* **9**, 16–33.

[35] Brooks, A. N. & Hughes, T. J. R. (1982) Streamline upwind/Petrov–Galerkin formulations for convection dominated flows with particular emphasis on the incompressible Navier–Stokes equations. *CMNA* **32**, 199–259.

[36] Burgreen, G. W., Antaki, J. F., Wu, Z. J. & Holmes, A. J. (2001) Computational fluid dynamics as a development tool for rotary blood pumps. *Artif. Organs* **25**(5), 336–340.

[37] Chan, W. K., Wong, Y. W., Ding, Y., Chua, L. P. & Yu, S. C. M. (2002) Numerical investigation of the effect of blade geometry on blood trauma in a centrifugal blood pump. *Artif. Organs* **26**(9), 785–793.

[38] Chan, W. K., Wong, Y. W., Ong, W., Koh, S.-Y. & Chong, V. (2005) Numerical investigation of the effects of the clearance gap between the inducer and impeller of an axial blood pump. *Artif. Organs* **29**(3), 250–258.

[39] Chien, S. (1970) Shear dependence of effective cell volume as determinant of blood viscosity. *Science* **168**, 977–979.

[40] Chien, S., Usami, S., Dellenback, R. J. & Gregersen, M. I. (1967) Blood viscosity: Influence of erythrocyte aggregation. *Science* **157**, 827–829.

[41] Chien, S., Usami, S., Dellenback, R. J. & Gregersen, M. I. (1967) Blood viscosity: Influence of erythrocyte deformation. *Science* **157**, 829–831.

[42] Coronado, O. M., Arora, D., Behr, M. & Pasquali, M. (2006) Four-field Galerkin/least-squares formulation for viscoelastic fluids. *J. Non-Newton. Fluid Mech.* **140**, 132–144.

[43] Couillette, C. & Pozrikidis, C. (1998) Motion of an array of drops through a cylindrical tube. *J. Fluid Mech.* **358**, 1–28.

[44] Cristini, V. & Kassab, G. S. (2005) Computer modeling of red blood cell rheology in the microcirculation: a brief overview. *Ann. Biomed. Eng.* **33**, 1724–1727.

[45] Crochet, M. J., Davies, A. R. & Walters, K. (1984) *Numerical Simulation of Non-Newtonian Flow,* Elsevier, New York.

[46] Curtas, A. R., Wood, H. G., Allaire, P. E., McDaniel, J. C., Day, S. W. & Olsen, D. B. (2002) Computational fluid dynamics modeling of impeller designs for the HeartQuest left ventricular assist device. *ASAIO* **48**, 552–561.

[47] Curtis, J. J. & Wagner-Mann, C. (2000) *Cardiac Assist Devices*, Futura, Armonk, NY.
[48] Davie, E. W. (2005) A brief historical review of the waterfall/cascade of blood coagulation. *J. Biol. Chem.* **278**, 50819–50832.
[49] Day, S. W., & McDaniel, J. C. (2005) PIV measurements of flow in a centrifugal blood pump: Time varying flow. *ASME* **127**, 254–263.
[50] De Wachter, D. & Verdonck, P. (2002) Numerical calculation of hemolysis levels in peripheral hemodialysis cannulas. *Artif. Organs* **26**(7), 576–582.
[51] DeBakey, M. E. (2000) The odyssey of the artificial heart. *Artif. Organs* **24**(6), 405–411.
[52] Ding, W. & Nakamura, S. (1998) Three-dimensional single passage simulation for the IVAS centrifugal heart pump. In: *Proceedings of 1998 ASME Fluids Engineering Division Summer Meeting*. June 21–25, Washington, DC, ASME.
[53] Easthope, P. L. & Brooks, D. E. (1980) A comparison of rheological and constitutive functions for whole human blood. *Biorheology* **17**, 235–247.
[54] Eckmann, D. M. (2000) Hematocrit, volume expander, temperature, and shear rate effects on blood viscosity. *Anesth. Analg.* **91**, 539–545.
[55] Eggleton, C. D. & Popel, A. S. (1998) Large deformation of red blood cell ghosts in a simple shear flow. *Phys. Fluids* **10**(8), 1834–1845.
[56] Evans, E. A. & LaCelle, P. L. (1975) Intrinsic material properties of the erythrocyte membrane indicated by mechanical analysis of deformation. *Blood* **45**, 29–43.
[57] Franca, L. P. & Frey, S. L. (1992) Stabilized finite element methods: II. The incompressible Navier-Stokes equations. *CMAME* **99**, 209–233.
[58] Franca, L. P., Frey, S. L. & Hughes, T. J. R. (1992) Stabilized finite element methods. Part I. Application to the advective-diffusive model. *CMAME* **95**, 253–276.
[59] Fung, Y. C. *Biomechanics: Mechanical Properties of Living Tissue,* Springer, New York.
[60] Gauthier, F. J., Goldsmith, H. L. & Mason, S. G. (1972) Flow of suspensions through tubes. Part X. Liquid drops as models of erythrocytes. *Biorheology* **9**, 205–224.
[61] Gawaz, M. P. (1856) *Das Blutplättchen.* Medinger Sohn, Frankfurt.
[62] Giersiepen, M., Wurzinger, L. J., Opitz, R. & Reul, H. (1990) Estimation of shear stress-related blood damage in heart valve prostheses: *In vitro* comparison of 25 aortic valves. *Int. J. Artif. Organs* **13**(5), 300–306.
[63] Gijsen, F. J. H., van de Vosse, F. N. & Janssen, J. D. (1999) The influence of the non-Newtonian properties of blood on the flow in large arteries: Steady flow in a carotid bifurcation model. *J. Biomech.* **32**, 601–608.
[64] Goubergrits, L. & Affeld, K. (2004) Numerical estimation of blood damage in artificial organs. *Artif. Organs* **28**(5), 499–507.
[65] Grigioni, M., Daniele, C., Morbiducci, U., D'Avenio, G., Di Benedetto, G. & Barbaro, V. (2004) The power-law mathematical model for blood damage prediction: Analytical developments and physical inconsistencies. *Artif. Organs* **28**(5), 467–475.
[66] Grmela, M. & Carreau, P. J. (1987) Conformation tensor rheological models. *J. Non-Newton. Fluid Mech.* **23**, 271–294.
[67] Gu, L. & Smith, W. A. (2005) Evaluation of computational models for hemolysis estimation. *ASAIO* **51**, 202–207.
[68] Guénette, R., Abdelmalek, Z., Fortin, A., Carreau, P. & Grmela, M. (1992) Simulation of viscoelastic flows using a conformation tensor model. *J. Non-Newton. Fluid Mech.* **45**, 187–208.
[69] Han, S., Marseille, O., Gehlen, C. & Blümich, B. (2001) Rheology of blood by NMR. *J. Magn. Reson.* **152**, 87–94.
[70] Hellums, J. D. & Brown, C. H., III. Blood cell damage by mechanical forces. In: N. H. C Hwang & N. A. Normann (editors), *Cardiovascular Flow Dynamics and Measurements*, University Park Press, Baltimore, MD, pp. 799–823..
[71] Hénon, S., Lenormand, G., Richert, A. & Gallet, F. (1999) A new determination of the shear modulus of the human erythrocyte membrane using optical tweezers. *Biophys. J.* **76**, 1145–1151.

[72] Hetzer, R., Müller, J., Weng, Y., Wallukat, G., Spiegelsberger, S. & Loebe, M. (1999) Cardiac recovery in dilated cardiomyopathy by unloading with a left ventricular assist device. *Ann. Thorac. Surg.* **68**, 742–749.

[73] Heuser, G. & Opitz, R. (1980) A Couette viscometer for short time shearing of blood. *Biorheology* **17**, 17–24.

[74] Ho, K. K., Anderson, K.M., Kannel, W. B., Grossman, W. & Levy, D. (1993) Survival after the onset of congestive heart failure in Framingham heart study subjects. *Circulation* **88**, 107–115.

[75] Hoffmann, J. I. & Christianson, R. (1978) Congenital heart disease in a cohort of 19,502 births with long-term follow-up. *Am. J. Cardiol.* **42**(4), 641–647.

[76] Hughes, T. J. R., & Brooks, A. N. (1979) A multi-dimensional upwind scheme with no crosswind diffusion. In: T. J. R. Hughes (editor), *Finite Element Methods for Convection Dominated Flows*, vol. 34, ASME, New York, pp. 19–35.

[77] Hughes, T. J. R., Franca, L. P. & Hulbert, G. M. (1989) A new finite element formulation for computational fluid dynamics. Part 8. The Galerkin/least-squares method for advective–diffusive equations. *CMAME* **73**, 173–189.

[78] Hulsen, M. A., Fattal, R. & Kupferman, R. (2005) Flow of viscoelastic fluids past a cylinder at high Weissenberg number: Stabilized simulations using matrix logarithms. *J Non-Newton. Fluid Mech.* **127**, 27–39.

[79] Johnson, W. (1973) *Engineering Plasticity,* VNR, London.

[80] Kameneva, M. V., Burgreen, G. W., Kono, K., Repko, B., Antaki, J. F. & Umezu, M. (2004) Effects of turbulent stresses upon mechanical hemolysis: Experimental and computational analysis. *ASAIO J.* **50**(5), 418–423.

[81] Keunings, R. (2001) Advances in the computer modeling of the flow of polymetric liquids. *Comput. Fluid Dyn.* **9**, 448–458.

[82] Klaus, S., Paul, R., Mottaghy, K., Reul, H. & Glasmacher, B. (2001) Investigation of flow and material induced hemolysis with a Couette type high shear system. *Materialwissenschaft Werkzeugtech.* **32**, 922–925.

[83] Knierbein, B., Reul, H., Eilers, R., Lange, M., Kaufmann, R. & Rau, G. (1992) Compact mock loops of the systemic and pulmonary circulation for blood testing. *Int. J. Artif. Organs* **15**(1), 40–48.

[84] Lee, S. S., Ahn, K. H., Lee, S. J., Sun, K., Goedhart, P. T. & Hardeman, M. R. (2004) Shear induced damage of red blood cells monitored by the decrease of their deformability. *Korea–Aust. Rheol. J.* **16**(3), 141–146.

[85] Leuprecht, A. & Perktold, K. (2001) Computer simulation of non-Newtonian effects on blood flow in large arteries. *Comp. Meth. Biomech. Biomed. Eng.* **4**, 149–163.

[86] Leverett, L. B., Hellums, J. D., Alfrey, C. P. & Lynch, E. C. (1972) Red blood cell damage by shear stress. *Biophys. J.* **12**, 257–273.

[87] Maffettone, P. L. & Minale, M. (1998) Equation of change for ellipsoidal drops in viscous flow. *J. Non-Newton. Fluid Mech.* **78**, 227–241.

[88] Masuzawa, T., Tsukiya, T., Endo, S., Tatsumi, E., Taenaka, Y., Takano, H., Yamane, T., Nishida, M., Asztalos, B., Miyazoe, Y., Ito, K., Sawairi, T. & Konishi, Y. (1999) Development of design methods for a centrifugal blood pump with a fluid dynamic approach: Results in hemolysis tests. *Artif. Organs* **23**(8), 757–761.

[89] Minami, K., Schulte-Eistrup, S., El-Banayosy, A. & Koerfer, R. (2004) Impact of regulatory affairs on the development of artificial organs, particularly ventricular assist devices. *Artif. Organs* **25**(5), 860–864.

[90] Mitoh, A., Yano, T., Sekine, K., Mitamura, Y., Okamoto, E., Kim, D., Yozu, R. & Kawada, S. (2003) Computational fluid dynamics analysis of an intra-cardiac axial flow pump. *Artif. Organs* **27**(1), 34–40.

[91] Miyazoe, Y., Sawairi, T., Ito, K., Konishi, Y., Yamane, T., Nishida, M., Asztalos, B., Masuzawa, T., Tsukiya, T., Endo, S. & Taenaka, Y. (1999) Computational fluid dynamics

analysis to establish the design process of a centrifugal blood pump: Second report. *Artif. Organs* **23**(8), 762–768.

[92] Murakami, T., Golding, L. R., Jacobs, G., Takatani, S., Sukalac, R., Harasaki, H. & Nosé, Y. (1979) Nonpulsatile biventricular bypass using centrifugal blood pumps. *Jap. Soc. Artif Organs* **8**, 636–639.

[93] Nakamura, S. (1997) Options and selection of numerical algorithms for unsteady incompressible Navier--Stokes equations. *Proceedings of the ASME Fluid Engineering Division Summer Meeting, FEDSM97-3666*, New York: American Society of Mechanical Engineers.

[94] Nakamura, S. & Yano, K. (1999) Computational simulation of flows in an entire centrifugal blood pump. *Artif. Organs* **23**(6), 572–575.

[95] Ng, B. T., Chan, W. K. & Li, H. D. (2000) Experimental and computational studies of the relative flow field in a centrifugal pump. *Crit. Rev. Biomed. Eng.* **28**(1), 119–125.

[96] Nonaka, K., Linneweber, J., Ichikawa, S., Yoshikawa, M., Kawahito, S., Mikami, M., Motomura, T., Ishitoya, H., Nishimura, I., Oestmann, D., Glueck, J., Schima, H., Wolner, E., Shinohara, T. & Nosé, Y. (2001) Development of the Baylor Gyro permanently implantable centrifugal blood pump as a biventricular assist device. *Artif. Organs* **25**(9), 675–682.

[97] Nosé, Y. (1998) Design and development strategy for the rotary blood pump. *Artif. Organs* **22**(6), 438–446.

[98] Nosé, Y. (2005) Is it a mistake to develop a totally implantable blood pump for destination therapy? *Artif. Organs* **29**(2), 93–94.

[99] Nosé, Y., Yoshikawa, M., Murabayashi, S. & Takano, T. (2000) Development of rotary blood pump technology: Past, present, and future. *Artif. Organs* **24**(6), 412–420.

[100] Okamoto, E., Hashimoto, T. & Inoue, T. (2003) Blood compatible design of a pulsatile blood pump using computational fluid dynamics and computer-aided design and manufacturing technology. *Artif. Organs* **27**(1), 61–67.

[101] Olsen, D. B. (1999) Rotary blood pumps: A new horizon. *Artif. Organs* **23**(8), 695–696.

[102] Olsen, D. B. (2000) The history of continuous-flow blood pumps. *Artif. Organs* **24**(6), 401–404.

[103] Owens, R. G. (2006) A new microstructure-based constitutive model for human blood. *J. Non-Newton. Fluid Mech.* **140**:57–70.

[104] Owens, R. G. & Phillips, T. N. (2002) *Computational Rheology,* Imperial College Press, London.

[105] Papantonis, D. (1991) Numerical prediction of the shear stresses and the mean exposure time for radial flow impellers. In: Thoma, Schima (editor), *Proceedings of the International Workshop on Rotary Blood Pumps*, Vienna, pp. 63–69.

[106] Papantonis, D. & Croba, D. (1988) Numerical calculation of the performances and shear stresses developed on centrifugal blood pumps. In: Thoma, Schima (editor), *Proceedings of the International Workshop on Rotary Blood Pumps*, Vienna, pp. 53–59.

[107] Pasquali, M. & Scriven, L. E. (2002) Free surface flows of polymer solutions with models based on the conformation tensor. *J. Non-Newton. Fluid Mech.* **108**, 363–409.

[108] Pasquali, M. & Scriven, L. E. (2004) Theoretical modeling of microstructured liquids: A simple thermodynamic approach. *J. Non-Newton. Fluid Mech.* **120**, 101–135.

[109] Perktold, K., Karner, G., Leuprecht, A. & Hofer, M. (1999) Influence of non-Newtonian flow behavior on local hemodynamics. *Z. Angew. Math. Mech.* **79**, 187–190.

[110] Pinotti, M. & Rosa, E. S. (1991) CFD simulation on the performance of parallel corotating disks as a heart assist device. In: *Proceedings of the Sixth Mediterranean Conference on Medical and Biological Engineering*, Capri, Italia: International Federation of Medical and Biological Engineering, V. 1, pp. 429–432.

[111] Pinotti, M. & Rosa, E. S. (1995) Computational prediction of hemolysis in a centrifugal ventricular assist device. *Artif. Organs* **19**(3), 267–273.

[112] Pozrikidis, C. (2003) *Modeling and Simulation of Capsules and Biological Cells,* Chapman Hall, Boca Raton, FL.

[113] Pozrikidis, C. (2004) Numerical simulation of cell motion in tube flow. *Ann. Biomed. Eng.* **33**, 165–178.

[114] Pozrikidis, C. (2003) Numerical simulation of the flow-induced deformation of red blood cells. *Ann. Biomed. Eng.* **31**, 1194–1205.

[115] Qian, Y. & Bertram, C. D. (2000) Computational fluid dynamics analysis of hydrodynamic bearings of the VentrAssist rotary blood pump. *Artif. Organs* **24**(6), 488–491.

[116] Rose, E. A., Gelijns, A. C., Moskowitz, A. J., Heitjan, D. F., Stevenson, L. W., Dembitsky, W., Long, J. W., Ascheim, D. D., Tierney, A. R., Levitan, R. G. Watson, J. T., Meier, P., Ronan, N. S., Shapiro, P. A., Lazar, R. M., Miller, L. W., Gupta, L., Frazier, O. H., Desvigne-Nickens, P., Oz, M. C. & Poirier, V. L. for the Randomized Evaluation of Mechanical Assistance for the Treatment of Congestive Heart Failure (REMATCH) Study Group. (2001) Long-term use of a left ventricular assistance for end-stage heart failure. *New Engl. J. Med.* **345**, 1435–43.

[117] Rossi Neto, J. M. (2004) A dimensão do problema da insufficiência cardíaca do Brazil e do mundo. *Revista Soc. Cardiol. Estado São Paulo* **14**(1), 1–10.

[118] Saad, Y. & Schultz, M. (1986) GMRES: A generalized minimal residual algorithm for solving nonsymmetric linear systems. *SIAM J. Scient. Stat. Comput.* **7**, 856–869.

[119] Schaefer, E. J. (2002) Lipoproteins, nutrition, and heart disease. *Am. J. Clin. Nutr.* **75**, 191–212.

[120] Schmid-Schönbein, H. & Wells, R. (1969) Fluid drop-like transition of erythrocytes under shear. *Science* **165**(3890), 288–291.

[121] Scott, M. (2005) *The Modeling of Blood Rheology in Small Vessels. PhD Thesis,* Department of Applied Mathematics, University of Waterloo, Waterloo, ON, Canada.

[122] Secomb, T. W., Hsu, R. & Pries, A. R. (1998) A model for red blood cell motion in glycocalyx-lined capillaries. *Model. Physiol.* **274**, 1016–1022.

[123] Snabre, P. & Mills, P. (1996) Rheology of weakly flocculated suspensions of viscoelastic particles. *J. Phys. III France* **6**, 1835–1855.

[124] Song, X., Throckmorton, A., Wood, H. G., Antaki, J. & Olsen, D. B. (2004) Quantitative evaluation of blood damage in a centrifugal VAD by computational fluid dynamics. *ASME* **126**, 410–418.

[125] Song, X., Throckmorton, A. L., Untaroiu, A., Patel, S., Allaire, P. E., Wood, H. G. & Olsen, D. B. (2003) Axial flow blood pumps. *ASAIO* **49**(4), 355–364.

[126] Song, X., Wood, H. G., Day, S. W. & Olsen, D. B. (2003) Studies of turbulence models in a computational fluid dynamics model of a blood pump. *Artif. Organs* **27**(10), 935–937.

[127] Song, X., Wood, H. G. & Olsen, D. B. (2004) Computational fluid dynamics (CFD) study of the fourth generation prototype of a continuous flow ventricular assist device (VAD). *J. Biomed. Eng.* **126**, 180–187.

[128] Stepanoff, A. (1957) *Centrifugal and Axial Flow Pumps,* Krieger, New York.

[129] Sun, J., Smith, M. D., Armstrong, R. C. & Brown, R. A. (1999) Finite element method for viscoelastic flows based on the discrete adaptive viscoelastic stress splitting and the discontinuous Galerkin method: DAVSS-G/DG. *J. Non-Newton. Fluid Mech.* **86**, 281–307.

[130] Takatani, S. (2001) Can rotary blood pumps replace pulsatile devices? *Artif. Organs* **25**(9), 671–674.

[131] Takatani, S., Ozawa, K., Golding, L., Jacobs, G., Murakami, T., Valdes, F., Harasaki, H., Kiraly, R. & Nosé, Y. (1980) Comparative evaluation of nonpulsatile and pulsatile cardiac prostheses. *Trans. Am. Soc. Artif. Intern. Organs* **26**, 438–443.

[132] Takiura, K., Masuzawa, T., Endo, S., Wakisaka, Y., Tatsumi, E., Taenaka, Y. Takano, H. Yamane, T., Nishida, M., Asztalos, B., Konishi, Y., Miyazoe, Y. & Ito, K. (1998) Development of design methods of a centrifugal blood pump with in vitro tests, flow visualization, and computational fluid dynamics: Results in hemolysis tests. *Artif. Organs* **22**(5), 393–398.

[133] Tezduyar, T. E., Mittal, S., Ray, S. E. & Shih, R. (1992) Incompressible flow computations with stabilized bilinear and linear equal-order-interpolation velocity–pressure elements. *CMAME* **95**, 221–242.

[134] Throckmorton, A., Untaroiu, A., Allaire, P. E., Wood, H. G., Matherne, G. P., Lim, D. S., Peeler, B. B. & Olsen, D. B. (2004) Computational analysis of an axial flow pediatric ventricular assist device. *Artif. Organs* **28**(10), 881–891.

[135] Throckmorton, A. L., Wood, H. G., Day, S. W., Song, X., Click, P. C., Allaire, P. E. & Olsen, D. B. (2003) Design of a continuous flow centrifugal pediatric ventricular assist device. *Int. J. Artif. Organs*, **26**(11), 1015–1031.

[136] Thurston, G. B. (1979) Rheological parameters for the viscosity, viscoelasticity and thixotropy of blood. *Biorheology* **16**, 149–162.

[137] Ündar, A. (2004) Myths and truths of pulsatile and nonpulsatile perfusion during acute and chronic cardiac support. *Artif. Organs* **28**(5), 439–443.

[138] Untaroiu, A., Wood, H. G., Allaire, P. E., Throckmorton, A. L., Day, S., Patel, S. M., Ellman, P., Tribble, C. & Olsen, D. B. (2005) Computational design and experimental testing of a novel axial flow LVAD. *ASAIO* **51**, 702–710.

[139] Virchow, R. (1856) *Gesammelte Abhandlungen zur Wissenschaftlichen Medicin,* Medinger Sohn, Frankfurt.

[140] Watanabe, N., Karsak, O., Neudel, F., Kink, T., Apel, J., Fujimoto, T., Reul, H. & Takatani, S. (2001) Simulation of the BP-80 blood pump. *Artificial Organs* **25**(9), 733–739.

[141] Watanabe, N., Masuda, T., Iida, T., Kataoka, H., Fujimoto, T. & Takatani, S. (2005) Quantification of the secondary flow in a radial coupled centrifugal blood pump based on particle tracking velocimetry. *Artificial Organs* **29**(1), 26–35.

[142] Waugh, R. E. & Hochmuth, R. M. (1995) Mechanics and deformability of hematocytes. In: J. D. Bronzino (editor), *Handbook of Bioengineering*, CRC Press, Boca Raton, FL, pp. 474–486.

[143] Wood, H. G, Throckmorton, A. L., Untaroiu, A. & Song, X. (2005) The medical physics of ventricular assist devices. *Rep. Prog. Phys.* **68**, 545–576.

[144] Wootton, D. M. & Ku, D. N. (1999) Fluid mechanics of vascular systems, diseases, and thrombosis. *Annu. Rev. Biomed. Eng.* **1999.01**, 299–329.

[145] Wu, J., Antaki, J. F., Wagner, W. R., Snyder, T. A., Paden, B. E. & Borovetz, H. S. (2005) Elimination of adverse leakage flow in a miniature pediatric centrifugal blood pump by computational fluid dynamics-based design optimization. *ASAIO* **51**, 636–643.

[146] Wu, Y., Allaire, P. & Tao, G. (2003) An adaptive speed/flow controller for a continuous flow left ventricular asssist device. In: *Proceedings of the American Control Conference*, Denver, CO, IEEE.

[147] Wurzinger, L. J., Opitz, R. & Eckstein, H. (1986) Mechanical blood trauma: An overview. *Angeiologie* **38**(3), 81–97.

[148] Yamaguchi, T., Ishikawa, T., Tsubota, K., Imai, Y., Nakamura, M. & Fukui, T. (2006) Computational blood flow analysis – new trends and methods. *J. Biomech. Sci. Eng.* **1**, 29–50.

[149] Yamane, T., Asztalos, B., Nishida, M., Masuzawa, T., Takiura, K., Taenaka, Y., Konishi, Y., Miyazoe, Y. & Ito, K. (1998) Flow visualization as a complementary tool to hemolysis testing in the development of centrifugal blood pumps. *Artif. Organs* **22**(5), 375–380.

[150] Yamane, T., Miyamoto, Y., Tajima, K. & Yamazaki, K. (2004) A comparative study between flow visualization and computational fluid dynamic analysis for the Sun Medical centrifugal blood pump. *Artif. Organs* **28**(5), 458–466.

[151] Yano, K. & Nakamura, S. (1997) Flow simulation of the IVAS heart pump using a parallel computer, T3D. In *Proceedings of ASME Fluids Engineering Division Summer Meeting*, Vancouver, Canada, IEEE.

[152] Yano, T., Sekine, K., Mitoh, A., Mitamura, Y., Okamoto, E., Kim, D.-W., Nishimura, I., Murabayashi, S. & Yozu, R. (2003) An estimation method of hemolysis within an axial

flow blood pump by computational fluid dynamics analysis. *Artif. Organs* **27**(10), 920–925.

[153] Yasuda, T., Shimokasa, K., Funakubo, A., Higami, T., Kawamura, T. & Fukui, Y. (2000) An investigation of blood flow behavior and hemolysis in artificial organs. *ASAIO* **46**(5), 527–531.

[154] Yeleswarapu, K. K. *Evaluation of Continuum Models for Characterizing the Constitutive Behavior of Blood, PhD Thesis,* Department of Mechanical Engineering, University of Pittsburgh, Pittsburgh, PA.

[155] Yeleswarapu, K. K., Antaki, J. F., Kameneva, M. V. & Rajagopal, K. R. (1995) A mathematical model for shear-induced hemolysis. *Artif. Organs* **19**(7), 576–582.

[156] Yeleswarapu, K. K., Kameneva, M. V., Rajagopal, K. R. & Antaki, J. F. (1998) The flow of blood in tubes: Theory and experiments. *Mech. Res. Comm.* **25**(3), 257–262.

[157] Yoshikawa, M., Nonaka, K., Linneweber, J., Kawahito, S., Ohtsuka, G., Nakata, K., Takano, T., Schulte-Eistrup, S., Glueck, J., Schima, H., Wolner, E. & Nosé, Y. (2000). Development of the NEDO implantable ventricular assist device with Gyro centrifugal pump. *Artif. Organs* **24**(6), 459–467.

[158] Yozu, R., Golding, L. R., Jacobs, G., Harasaki, H. & Nosé, Y. (1985) Experimental results and future prospects for a nonpulsatile cardiac prosthesis. *World J. Surg.* **9**(1), 116–127.

[159] Yu, S. C. M., Ng, B. T. H., Chan, W. K. & Chau, L. P. (2000) The flow patterns within the impeller passage of a centrifugal blood pump model. *Med. Eng. Phys.* **22**, 381–393.

[160] Yuri, K., Iwahashi, H., Motomura, T., Hata, A., Asai, T., Nosé, Y., Arora, D., Behr, M. & Pasquali, M. (2004) ASAIO 50th anniversary conference abstracts: Different levels of hemolysis occurred by a centrifugal blood pump in various clinical conditions. *ASAIO J.* **50**(2), 121.

[161] Zhang, J., Gellman, B., Koert, A., Dasse, K. A., Gilbert, R. J., Griffith, B. P. & Wu, Z. J. (2006) Computational and experimental evaluation of the fluid dynamics and hemocompatibility of the CentriMag blood pump. *Artif. Organs* **30**(3), 168–177.

[162] Zhang, J. B. & Kuang, Z. B. Study on blood constitutive parameters in different blood constitutive equations. *J. Biomech.* **33**, 355–360.